THESIS FOR THE DEGREE OF DOCTOR OF PHILOSOPHY

EM Design for New Ultra Wide Band Technologies: Eleven Feed Baluns, Bowtie Antennas and Gap Waveguides

Syed Hasan Raza Zaidi

CHALMERS

Department of Signals and Systems
Antenna Group
Chalmers University of Technology
SE-41296 Göteborg, Sweden

Göteborg, 2014

EM Design for New Ultra Wide Band Technologies: Eleven Feed Baluns, Bowtie Antennas and Gap Waveguides

Syed Hasan Raza Zaidi

Copyright © Syed Hasan Raza Zaidi, 2014
All rights reserved

ISBN 978-91-7385-966-0
Doktorsavhandlingar vid Chalmers tekniska högskola
Ny serie nr: 3647
ISSN 0346-718X

Department of Signals and Systems
Antenna Group
Chalmers University of Technology
SE-412 96 Göteborg, Sweden
Telephone: +46 (0) 31 772 4830

Contact information:
Syed Hasan Raza Zaidi
Department of Signals and Systems
Chalmers University of Technology
Hörsalsvägen 11
S-412 96 Göteborg
Sweden
Telephone +46 (0)31 772 4830
Email: hasan.raza@chalmers.se

Printed in Sweden by Chalmers Reproservice
Göteborg, February, 2014

To my family

EM Design for New Ultra Wide Band Technologies: Eleven Feed Baluns, Bowtie Antennas and Gap Waveguides

SYED HASAN RAZA ZAIDI
Department of Signals and Systems
Chalmers University of Technology

Abstract

UWB (ultra wideband), depending on the application requirement, is usually referred to more than 500 MHz bandwidth for radio/wireless applications. Here in this thesis it is also used to denote extremely wideband antennas and components of several octaves bandwidth, particularly for high frequency applications. One of the critical parts of an UWB antenna is its feeding circuits, which should deliver the signal from the UWB antenna to LNAs with as small losses as possible. This is in particular important in future radio telescopes for SKA (Square Kilometer Array) and VLBI2010 (a Very Long Baseline Interferometry project), to avoid severe degradations of their low noise performance. The first part of this thesis is primarily associated with designing UWB baluns for the decade bandwidth Eleven feed, which is a candidate for use in large reflector antennas for SKA and VLBI2010 telescopes. The second topic of the thesis addresses a four-port dual polarized UWB bowtie antennas, an alternative simpler candidate for commercial UWB sensor and radar applications in the unlicensed 3-10 GHz frequency band. The third part deals with UWB waveguide components and antennas using the novel gap waveguide technology, mainly intended for millimeter and submillimeter wave applications such as radio links in V-, E-, and W-band covering 50-110 GHz. The gap waveguide is an UWB technology, because it inherently has a broader bandwidth than normal hollow waveguides and can be used over more than octave bandwidth. In addition, the gap waveguide is less dispersive than a normal hollow waveguide.

The decade bandwidth Eleven antenna can be considered to have either four differential ports or eight single-ended ports, and different ways of combining the eight ports are needed for different purposes and applications. The most feasible combination is that the antenna is fed by four baluns and two additional power dividers, to get dual-polarized directive beam suitable for feeding a reflector antenna. A balun is a device that transforms a balanced two-wire line to an unbalanced coaxial or microstrip line. The first part of the thesis presents a new passive balun solution for the Eleven antenna and a way to integrate four of these baluns together with the antenna in such a way that the four differential ports transform to four single-ended ports. It is also important to verify and evaluate the radiation efficiency of a multiport antenna before being integrated in the system. This thesis addresses how to measure the radiation efficiency of a multiport antenna excluding the losses in the feeding network used for the measurement, particularly when the impedance match between the antenna and the feeding network is not so perfect.

The new dual-polarized self-grounded bowtie antenna has many advantages. One of the characteristics of this antenna is its flexibility for different applications: a multi-port antenna in MIMO systems, a directional dual-polarized (linear or circular) antenna in radar or sensor

systems. The four-armed geometry of the antenna has been optimized in the design for the best impedance matching to 50 ohm coax over 1.5 – 3 GHz, an octave bandwidth, which is desired for a micro base transceiver station antenna.

The gap waveguide makes it possible to realize low loss circuits at millimeter and sub-millimeter waves, without the need of metal contact between joining metal pieces, a difficulty present when using normal hollow waveguides. The present work includes a study of the resemblance between the groove gap waveguide and the standard hollow rectangular waveguide, and between the ridge gap waveguide and the normal hollow ridge waveguide. The dispersion diagrams and characteristic impedances have been compared. These results are very useful for designing, simulating and measuring gap waveguide components of different kind, because they show under which conditions and accuracies standard waveguide interfaces can be used.

The new design of microstrip-ridge gap waveguide by using via holes in the PCBs, makes a solution for high frequency circuits. The present thesis also includes the study about pin sensitivity, losses, and a comparison of this type of gap waveguide with the performance of normal microstrip line and inverted microstrip lines. A WR-15 to microstrip-ridge gap waveguide transition has also designed. The results are verified with measurements on microstrip-ridge gap waveguides with WR15 transitions at both ends.

Finally, the thesis presents an UWB microstrip power divider that was designed and packaged using gap waveguide technology, and a ridge gap waveguide ring hybrid. The power divider has a bandwidth of 2–14 GHz, and it is intended to be used in the feed network for the Eleven feed.

Keywords: Ultra-wideband, Eleven feed, baluns, Multiport feeding network, gap waveguide, power divider, packaging, ring hybrid.

Contents

Abstract		i
Contents		iii
List of papers		v
Preface		vii
Acknowledgement		ix
1.	Introduction	1
2.	Overview of Balun Technology, self grounded bowtie antenna and the gap waveguide technology	7
3.	UWB balun feeding solution to the Eleven feed	13
4.	Dual Polarized Self-grounded Bowtie Antenna	27
5.	Numerical ports and characteristic impedance of gap waveguide	31
6.	Microstrip-Ridge Gap Waveguide – study of losses, bends and transition to WR-15	41
7.	UWB Power Divider, packaged with Gap Waveguide Technology	51
8.	Conclusion	55
Bibliography		57

List of papers

A. **H. Raza**, J. Yang, and M. Pantaleev, “Integration of ultra-wideband planar baluns into the Eleven feed”, IET Microwaves, Antennas & Propagation, Volume 8, Issue 1, 08 January 2014, pp. 22 – 28.

B. **H. Raza**, J. Yang, and A. Hussain, “Measurement of Radiation Efficiency of Multiport Antennas with Feeding Network Corrections”, IEEE Antennas and Wireless Propagation Letters, Vol. 11, pp. 89 - 92, 2012.

C. **H. Raza**, J. Yang and M. Pantaleev, “A compact UWB passive balun solution for cryogenic 2 – 13 GHz eleven feed for future wideband radio telescopes”, 5th Eur. Conf. On Antennas and Propagation (EuCAP 2011), Rome, Italy, 11 – 15 April 2011.

D. **H. Raza**, J. Yang, P.-S. Kildal, and E. Alfonso, “Resemblance between gap waveguides and hollow waveguides", IET Microwaves, Antennas & Propagation, Volume 7, Issue 15, 10 December 2013, pp. 1221 – 1227.

E. **H. Raza**, J. Yang, and P.-S. Kildal, “Study of the characteristic impedance of gap waveguide microstrip line realized with square metal pins”, 7th Eur. Conf. on Antennas and Propagation (EuCAP 2013), Göteborg, Sweden, 8 – 12 April 2013.

F. **H. Raza**, and J. Yang, “A Low Loss Rat Race Balun in Gap Waveguide Technology”, 5th Eur. Conf. On Antennas and Propagation (EuCAP 2011), Rome, Italy, 11 – 15 April 2011.

G. **H. Raza**, and J. Yang, “Compact UWB Power Divider Packaged by Using Gap-Waveguide Technology”, 6th Eur. Conf. On Antennas and Propagation (EuCAP 2012), Prague, Czech Republic, 26 – 30 March 2012.

H. **H. Raza**, J. Yang, P-S. Kildal and E. Alfonso, “Microstrip-Ridge Gap Waveguide – Study of Losses, Bends and Transition to WR-15”, submitted to Transactions on Microwave Theory and Techniques, 9th december, 2013.

I. **H. Raza**, A. Hussain, J. Yang and P.-S. Kildal, “Wideband Compact 4-port Dual Polarized Self-grounded Bowtie Antenna”, submitted to IEEE Transactions on Antennas and Propagation, 18th december, 2013.

Other related publications by the Author not included in this thesis:

- J. Yang, and **H. Raza**, “Empirical Formulas For Designing Gap-Waveguide Hybrid Ring Coupler”, Microwave and Optical Technology Letters, Vol. 55, Issue 8, pp. 1917–1920, August 2013.

- J. Yang, M. Pantaleev, T. Ekebrand, P.-S. Kildal, **H. Raza**, J. Yin, J. Jonsson, L. Helldner, A. Emrich, B. Klein, "Development of the Cryogenic 2-14 GHz Eleven Feed System for VLBI2010", 6th Eur. Conf. On Antennas and Propagation (EuCAP 2012), Prague, Czech Republic, 26 – 30 March 2012.

- S. Rahiminejad, A. U. Zaman, E. Pucci, **H. Raza**, V. Vassilev, S. Haasl, P. Lundgren, P.-S Kildal, P. Enokssona, "Design of Micromachined Ridge Gap Waveguides for Millimeter-Wave Applications", Proc. Eurosensors XXV, September 4-7, 2011, Athens, Greece.

- S. Rahiminejad, **H. Raza**, A. U. Zaman, S. Haasl, P. Enoksson, and P.-S. Kildal, "Micromachined Groove Gap Waveguides for 100 GHz applications", 7th Eur. Conf. on Antennas and Propagation (EuCAP 2013), Gothenburg, Sweden, 8-12 April 2013.

- P.-S. Kildal, X. Chen, **H. Raza**, M. Gustafsson, Z. Shen, "Characterization of a Wideband Compact 4-port Bowtie Antenna for Micro BTS in Rich Isotropic Multipath and random-LOS", submitted to IEEE Transactions on Antennas and Propagation, Dec. 2013.

Preface

This report is a thesis for the degree of Doctor of Philosophy at Chalmers University of Technology. The work is divided into three main parts: UWB balun solutions for the eleven feed, dual polarized self-grounded bowtie antenna and Wideband gap waveguide components. This work has been supported in parts by the Swedish Foundation for Strategic Research (SSF) within the Strategic Research Center CHARMANT, Pakistan's NESCOM scholarship program and partially by Swedish Research Council VR. My principle supervisor is Associate Prof. Jian Yang and Prof. Per-Simon Kildal is my examiner. The work was carried out between March 2010 and February 2014 at antenna group of Chalmers.

Acknowledgement

First and foremost, I would like to thank Prof. Per-Simon Kildal for accepting me as a PhD student in his group and for giving me the opportunity to work on creative projects like eleven feed, bowtie antenna and gap waveguide. He is a true inspiration for me. I would also like to thank my supervisor, Associate Prof. Jian Yang for his support and confidence in my work. His patience and encouragement were very useful to me throughout the course of this research.

I thank, from the bottom of my heart, to my office in Pakistan who have supported me three years at Chalmers with their true commitment.

I would like to acknowledge Dr. Miroslav Pantaleev for making baluns for Eleven feed and Ahmed, for helping me in doing measurements of the Eleven feed and bowtie antenna in reverberation chamber. Many thanks and gratitude to all the former and present members of the Antenna group, Prof. Jan Carlsson, Associate Prof. Mariana, Dr. Rob Maaskant, Dr. Chen, Dr. Ashraf, Oleg, Aidin, Dr. Esperanza, Erik and Carlo for making an excellent research environment.

My wife Sana's love and support, my son Kumail's patience and my little daughter Abeeha's smile contributed to my work more than one could ever imagine. Their smiles, love and support encourage me to achieve my career goals. Finally, with all my heart, I would like to thank my parents for always supporting me.

Syed Hasan Raza Zaidi
Göteborg, February 2014

Part- I

Introduction

Chapter 1

Introduction

UWB antennas are always being of interest because of the wide frequency range and multiple usages. The UWB technology has found many applications like in modern radar, electronic warfare (EW) systems, UWB sensor network for precise ranging and location, and short range communication systems. Although it is also possible to place several antennas to cover a few different bands in some systems, because of the restriction in payload, limited space, cost and electromagnetic interference (EMI) issues, integration of these antennas into a platform (such as aircraft/cars/trucks) is a challenge. Therefore, there is a need of ultra-wideband (UWB) antennas with a low profile, which have sufficient bandwidth to cover the desired operation bands [1].

There is no fixed definition on the bandwidth of a UWB antenna. It simply depends on the requirements of the system. The original FCC definition of UWB specifies 25 percent or more fractional bandwidth (-10 dB bandwidth to center frequency). In some cases the antenna's bandwidth is specify based on the frequency range where the reflection coefficient is less than e.g. -10 dB, whereas in other cases constant radiation pattern and directivity over the whole bandwidth [2] is required. If the main purpose of an antenna is to radiate in a desired direction it is logical to use realized gain and radiation pattern to define the bandwidth. In all general cases, the bandwidth of a UWB antenna is bounded by geometrical parameters. The highest frequency in the bandwidth is usually determined by the feeding mechanism whereas the low end of the bandwidth is limited by the maximum dimension of the aperture [1], [2]. So it is important to know how small an antenna can be in order to achieve the desire specification at the low end of the bandwidth, especially for low frequency applications.

There are mainly four ways of realizing UWB antennas, the scaled structure (such as bow-tie shaped dipoles, biconical dipoles and log-periodic dipole arrays), the self-complementary structure (self-complementary spiral antennas), the gradual-transition (Vivaldi antennas) and the multiple reflection (or resonance) structure (dielectric resonator antenna) [3], [4].

1.1 UWB balun feeding

Generally, a UWB antenna can have a broad frequency range, e.g. $2(f_h - f_l)/(f_h + f_l) > 0.2$ in order to be 'ultra wide' [5]. UWB antennas offer many desirable features, and at the same time often with a simple RF front-end. However high gain, high radiation efficiency and good impedance matching simultaneously across a wideband are real challenges for UWB antenna design. The feeding network design is a critical issue to meet these challenges, where a compact size, manufacturability with low cost, mechanical stability, low ohmic loss, and good matching performance are often required [6].

The first topic of this thesis discusses the feeding mechanism for an UWB antenna, the Eleven feed [7]-[14], see Figure 1.1, for high frequency applications, such as 1 – 10 GHz version for the Square Kilometer Array (SKA) project and the 2 – 14 GHz version for the Very Long Baseline Interferometer (VLBI2010) projects. The Eleven feed is a decade bandwidth log periodic dipole array antenna which has been developed at Chalmers University of Technology since 2005. It has been shown that the Eleven feed has good features, especially for the applications in radio telescopes. Compared to several other candidate feeds [15]-[17] for the SKA and the VLBI2010 projects, the Eleven feed has many advantages over them in terms of the size, low profile and simple geometry , constant phase center, nearly constant directivity, low cross-polar side lobe levels and moreover nearly constant beam width over decade bandwidth. In addition, the multi-port Eleven antenna has been studied for its versatility, such as for use in monopulse tracking systems [18] and UWB MIMO systems [19], [20]. However, the Eleven feed has more ports (total eight ports) than other candidates, which requires more low-noise amplifiers (LNAs) in the whole antenna system. Therefore, different feeding networks for the antenna have been suggested along with different combinations of them, where the passive balun solution is an attractive one [21], [22].

An antenna with a balanced input port, such as a dipole, requires a transition to a more convenient transmission line, such as a coaxial line or a microstrip line, i.e. from the balanced transmission line to an unbalanced transmission line [23]. In the balanced line there is no net current flow through the grounded shield, i.e. $I_{surf} = 0$, in the ideal case, see Figure 1.2. If the net surface current is not equal to zero, it indicates that common modes are excited, which always needs to be avoided in balun design. Usually the bandwidth of an antenna is limited by that of the balun used for the antenna.

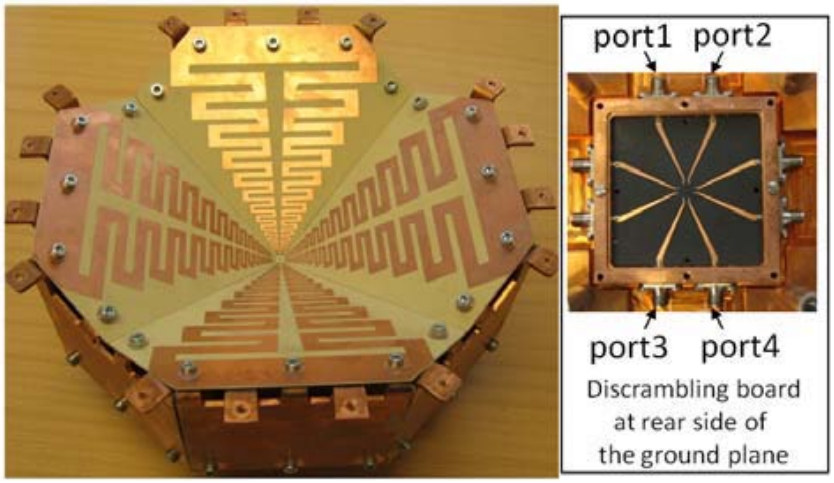

Figure 1.1: Photo of the manufactured Eleven feed, and the descrambling board at the rear side of the ground plane [22].

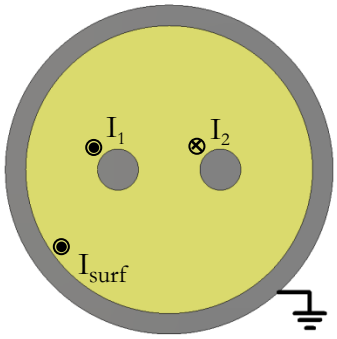

Figure 1.2: Shielded two wire balanced transmission line

1.2 UWB MIMO antenna

Many researchers have focused on wideband multiple-input-multiple-output (MIMO) antennas [24], [25]. MIMO allows several transmitting and receiving antennas that operate simultaneously. The UWB MIMO functioning over a wide frequency range helps to receive multipath propagation with non-line-of-sight (NLOS), eventually resulting in the attainment of more accurate data. However, challenges in development of UWB MIMO antennas needs to be resolved to enhance the effectiveness of MIMO [26], [27]. These challenges include low mutual coupling, low correlation, high diversity gain, and low input refection coefficient.

The second topic of this thesis is therefore devoted to the design and development of a multi-port UWB MIMO antenna that is characterized both for operation in multipath and under so called random LOS.

1.3 UWB Components at higher frequencies

Just like as UWB antennas, the design of wideband components especially at higher GHz is not an easy task either. Generally, the circuits suffer from the losses in the transmission lines, where the losses due to conductor are more significant than the losses due to dielectric materials and their packaging is a real challenge. The third topic of this thesis deals with the developments of wideband gap waveguide components.

The gap waveguide is a new planar microwave circuit technology which was originally proposed by P.-S. Kildal [28], see Figure 1.3. This waveguide aims to make low loss circuits at mm and sub-mm wave, particularly above 60 GHz, because the waveguide can be made by only metals. By using conventional rectangular waveguide, the tolerance requirements are difficult to meet and the metal contact for the waveguide walls imposes a difficulty for manufacturing. By using microstrip type transmission line, the loss in the dielectrics is often unacceptable. Moreover, the gap waveguide technology can be used for packaging of the microstrip circuits for suppressing the unwanted radiations without having any cavity resonances over a wide bandwidth. There is also a special advantage in gap waveguide of realizing practically useful packaged **inverted microstrip lines [29]**. Such microstrip gap waveguide line is realized by having a dielectric layer over a periodic pattern of pins, and there is an air gap between the top metal plate and the substrate material supporting the microstrip line. The pin structure works as an artificial magnetic surface (AMC), so the microstrip gap waveguide is an AMC-packaged inverted (or suspended) microstrip line. This is a new method to make a microstrip line in gap waveguide technology. In this thesis we present the design and development of 'microstrip-ridge gap waveguide' using via holes as the periodic pins at 60 GHz.

One of basic problems while simulating gap waveguide structure in commercial electromagnetic solvers is how to model the ports for gap waveguide in order to have accurate and fast simulations. A numerical study on the modeling of the gap waveguide port is presented in the thesis, with a method to estimate the characteristic impedance of the gap waveguide from the reflection coefficient.

1.4 Outline of the Thesis

A brief overview of various balun techniques for UWB antennas in literature, introduction to UWB bow-tie antenna and a basic summary of the new gap-waveguide technology are presented in Chapter 2, offering an understanding of the context of my work in developments of UWB balun, self-grounded bow-tie antenna and gap-waveguide components. Chapter 3 discusses a planar UWB balun solution to the Eleven antenna. Design of the multi-port self-grounded bow tie antenna is presented in Chapter 4. Numerical study on ports for simulating the gap waveguide circuits is described in Chapter 5. Chapter 6 presents a transition of microstrip-ridge gap waveguide to WR-15 standard rectangular waveguide at 60 GHz. Chapter 7 shows wideband power divider by using gap waveguide technology. The conclusion ends the first part of the thesis. The second part consists of nine papers, which is the basis of this thesis.

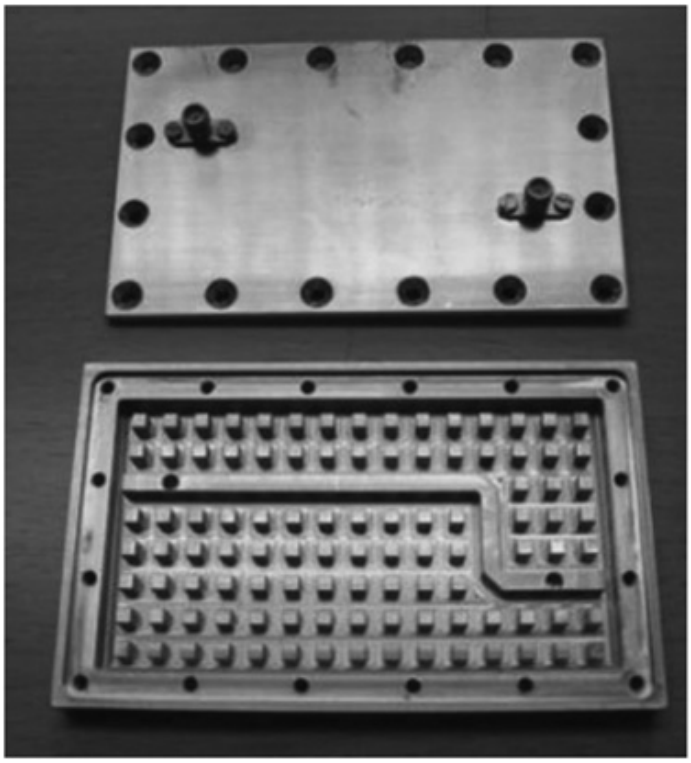

Figure 1.3: Photo of the 12–18 GHz demonstrator designed and measured for verifying the ridge gap waveguide technology [30].

Chapter 2

Overview of Balun Technology, self grounded bow-tie antenna and the gap waveguide technology

2.1 Overview of Balun Technology

Antennas, if not fed properly; do not work as predicted by the design. Many antennas require balanced-line feeding, while power/signal transmission is mostly carried out by unbalanced line. Therefore, a balanced-to-unbalanced transformer, a balun, is a key issue in antenna design.

To design a UWB balun is a challenge. A lot of wideband balun designs have been published [31]-[38] and some of them are summarized below and in Table 2.1.

Log-periodic balun is an octave bandwidth balun. The design and structure is based on the log-periodic antenna theory [31]. The bandwidth is depending on the number of sections of resonators. This structure is big in size so it is difficult to accommodate four baluns of such type on the back of the Eleven feed. There is another wide-band microstrip balun implemented on a single-layer printed circuit board consisting of a wide-band Wilkinson power divider and a non coupled-line broad-band 180° phase shifter [32]. The 10-dB return loss of this balun has been achieved across the bandwidth from 1.7 GHz to 3.3 GHz, or 64%. Due to this only octave bandwidth limitation, this balun is not suitable for decade bandwidth Eleven feed. Broadband phase shifting following the Wilkinson power divider in the above design can also be achieve if a 3 dB 90° hybrid coupler [33] is used with the coupled and transmitted port being short circuited or open circuited. It was shown that this balun performed well within 5-11 GHz band. Again the bandwidth, achieved by this balun, is not satisfactory according to the Eleven feed requirement. The only attractive balun on single layer PCB fulfilling requirements of Eleven feed is the marchand balun [34]. This balun has 11:1 bandwidth with less than 3° maximum phase imbalance. However, in [34] results show that it has high losses as well as the S_{11} is not less than -10 dB.

UWB out-of-phase power divider, utilizing both sides of PCB [35], can also be used to feed antenna. This design is based in the transformation from microstrip to slot line and then again slot line to the two arms of microstrip line making out-of-phase power divider. It is shown that the -10 dB reflection coefficient is between 3–11 GHz with about 1 dB transmission loss. Similarly, there is another three layer PCB design for out-of-phase power division based on parallel strip line to microstrip line transition [36] making the output ports on opposite side of middle layer. The output ports are not in the same plane. The performance of this is similar to that of the previous one. The decade bandwidth balun based on microstrip-to-coplanar stripline transition presented in [37] has a good matching performance but with a high transmission loss. The microstrip-to-parallel stripline transition presented in [38] is a simple design and easy to manufacture. Our work is to investigate different tapering techniques to obtain a better performance with a more compact size.

Table 2.1 Wideband Baluns in Literature

		Bandwidth, Phase Imbalance	Size [for 1 GHz]	Comments
Log – Periodic balun [31]	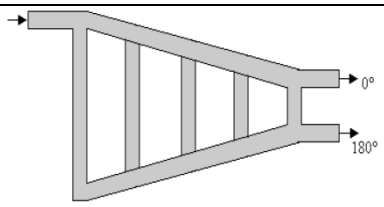	~ 67 % or 2:1 From 1.8–3.8 GHz ± 10°	57 mm x 100 mm	Large structure
Broadband power divider followed by delay line phase shifter [32]	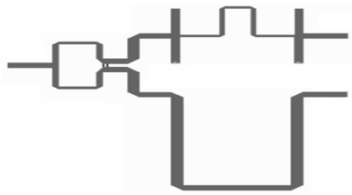	64 % or 2:1 From 1.7–3.3 GHz ± 5°	70 mm x 70 mm	Large structure
Broadband power divider followed by coupled line phase shifter [33]	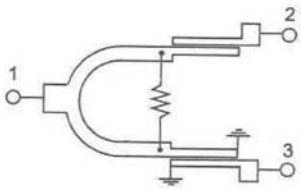	75% From 5–11 GHz ± 7°	56 mm x 30 mm	Very complex structure.

Marchand balun [34]	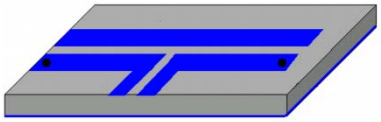	~ 167% or 11:1 From 2–22 GHz ± 3°	Size not specified	Multi layers High losses & S_{11} higher than -10 dB
UWB out of phase power divider [35]	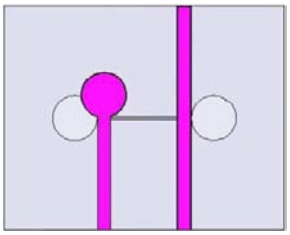	115% or ~ 4:1 From 3–11 GHz ±0.25°	40 mm x 20 mm	Large area requires to bend the output ports.
UWB out of phase power divider [36]	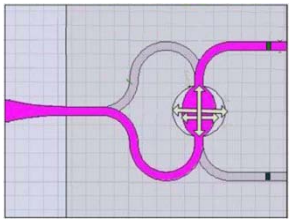	115% or ~ 4:1 From 3 – 11 GHz ±0.5°	20 mm x 20 mm	Large area require to bend the output ports.
UWB Microstrip to CPS transition [37]	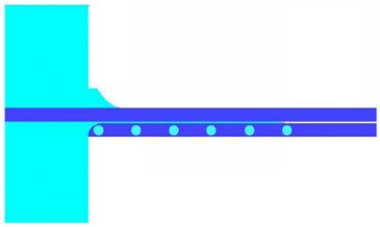	10:1 From 4 – 40 GHz	63.5 mm length	Large structure and difficult to package it inside.
Microstrip to paralle stripline transition [38]	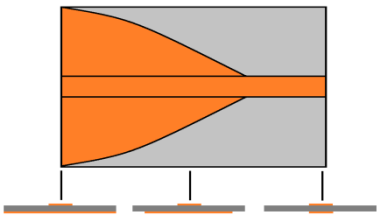	10:1 From 1.5 – 15 GHz	60 mm length	Large structure and difficult to package it inside.

2.2 Introduction to Self-grounded bowtie antenna

The first design of self-grounded bowtie antenna was presented in [39], [40], where the aim is to make a directional UWB antenna with low-profile and having many advantages, such as low interference level, high penetration ability and compact geometrical configuration. This is remarkable, as most of the small UWB antennas are omni-directional in radiation characteristics, for example, Bow-tie dipole

[41]. The directional UWB antennas are mainly traveling-wave structure having high-profile, such as Vivaldi antennas [42] and Lindgren horn [43].

The geometrical configuration of the self-grounded bowtie antenna is shown in Figure 2. 1. A tilted infinite bowtie dipole is located above a ground plane. The antenna, then become a frequency independent antenna with directional radiation characteristics due to this configuration. However, the structure should be truncated and the truncation is done by connecting the radiating element to the ground plan at the outer end of the antenna. That is why this antenna is referred to as the self-grounded bowtie. This antenna has a simple geometry; reflection coefficient is lower than -10 dB over the frequency range of 2-15 GHz and having stable radiation beams normal to the ground plane.

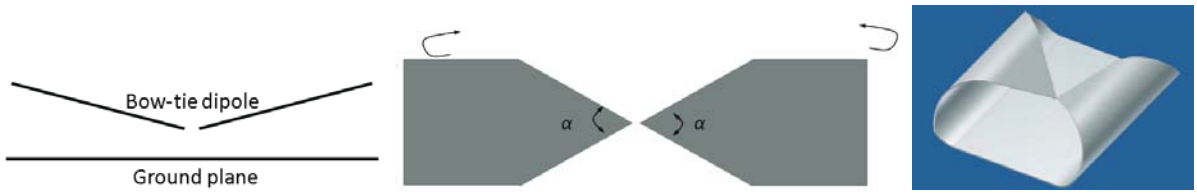

(a) (b) (c)

Figure 2. 1 Basic geometry and configuration of the bowtie antenna [39].

2.3 Introduction to Gap Waveguide

Gap waveguide technology is a new technique to make low loss circuits at millimeter and sub-millimeter waves [28]. The waveguide can be realized without having any dielectric material inside it, and there is no need to have electrical contact between the top and the bottom metal plates, the latter being provided with pins (or rather posts). These pins create a periodic metal texture that blocks parallel-plate waves to propagate everywhere except along a metal ridge or groove between the pins. The bandwidth of this particular behavior is referred to as a parallel-plate stopband. This stopband makes it also possible to use the gap waveguide technology for packaging of both passive and active microwave circuits realized in other technologies such as microstrip and co-planar waveguides [44], [45].

The basic theory of this new type of waveguide can be described as follows. One of the parallel plates is textured by periodic structures, preferably in the form of rectangular shapes. These periodic structures produce artificially high surface impedance, ideally Perfect Magnetic Conductors (PMC), and

together with a smooth metal plate on the top of them they generate a stopband for parallel-plate modes. If there is a metallic ridge or groove within this periodic texture and the distance between the top metal plate and the periodic structure is less than the quarter wavelength, only fundamental mode (quasi TEM mode in ridge gap waveguide and TE_{10} mode in case of groove gap waveguide) can propagate along the ridge or the groove [46], as illustrated in Figure 2.2. For this reason this type of waveguide is called as gap waveguide. The important parameters for defining the stopband are the period of pin structure, the length of air gap between the top of pins and upper smooth plate, and the height and the width of pins [47]. The height of pins is usually set as the quarter wavelength at the center frequency of the stopband. Note that the air gap must be smaller than quarter wavelength [47] and width of the pin plus the distance between two pins must be less than half the wavelength.

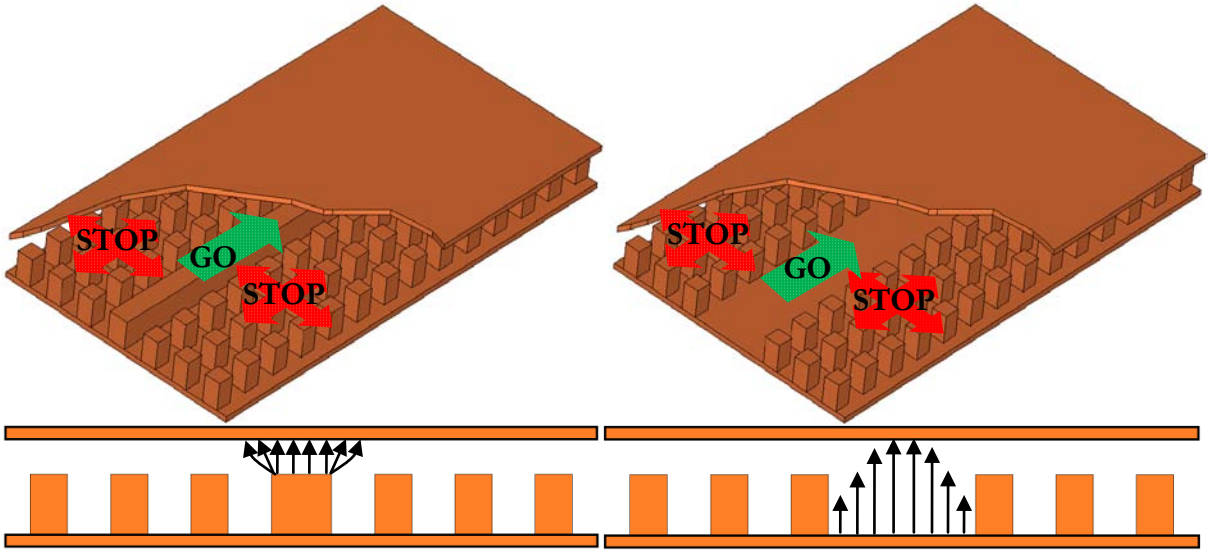

Figure 2.2: Front and top view of basic structures of ridge gap waveguide (left) and groove gap waveguide (right) depicting the propagation region.

With the presence of air gap, i.e. without having any dielectric material and only metal involve everywhere, both the ridge and the groove gap waveguides have lower loss than microstrip lines. The advantage of the gap waveguide compared to normal hollow waveguides is that the latter is difficult to manufacture at high frequency. The normal procedure is that the hollow waveguides and waveguide components are manufactured from two metal pieces and they must be joined with a good metal contact everywhere between them, which is difficult, whereas this is not needed for the gap waveguides.

Chapter 3

UWB balun feeding solution to the Eleven feed

Orientation of the balun on the back of Eleven feed is shown in Figure 3.1, where baluns are just represented by a symbolic box at this stage. With this configuration, the box of the balun can be replaced by any type of the first four baluns described in Table 2.1. But most of them are of octave bandwidth, whereas requirement of Eleven feed is decade bandwidth balun. So these baluns can't be used as for feeding of the Eleven antenna. Although there are some designs available based on Marchand balun [34] having bandwidth of about 11:1, the insertion loss is about 2 dB and S_{11} is higher than -10 dB over most of bandwidth. Similarly other designs in the Table 2.1 are available, based on transition from microstrip to other types of transmission line. This involves utilization of both sides of PCBs. So they can't be arrange on the back of Eleven feed, in the orientation shown in Figure 3.1, because there will be ground wall on one side.

Microstrip to stripline transition as shown in Figure 3.2, usually achieves more than decade bandwidth [38]. They are easy to manufacture and several tapering techniques are available to match the low impedance unbalance line with a high impedance balanced lines. Due to low losses and broad bandwidth nature, this balun can be a suitable candidate for the Eleven feed. Orientation of this type of balun is shown in Figure 3.3 where it is connected to Eleven feed petal vertical to the ground plane. This type of arrangement requires solid metallic frames to hold them stably. Those frames may cause resonances at some frequency points which can't be avoided. Similarly, when the balun will pass through the hole of ground plane to connect to the feed petal, this may also generate the common modes.

An ideal balun generates a fully differential mode at the output of the balanced port. The performance of the balun can be described by a three port scattering matrix, as shown by the Figure 3.4, where Port 1 is the unbalance port, and Ports 2 and 3 are the two output balanced ports of the balun. The important parameters for describing the performance of balun are (1) the reflection coefficient, (2) ohmic losses and (3) Common – mode rejection ratio (CMRR) $(S_{31} - S_{21})/(S_{31} + S_{21})$. The common–mode is rejected if S_{31} is equal to S_{21} in magnitude and 180° out of phase with respect

to S_{21}. An ideal balun has a fully differential mode at the output, i.e., the common-mode is totally rejected.

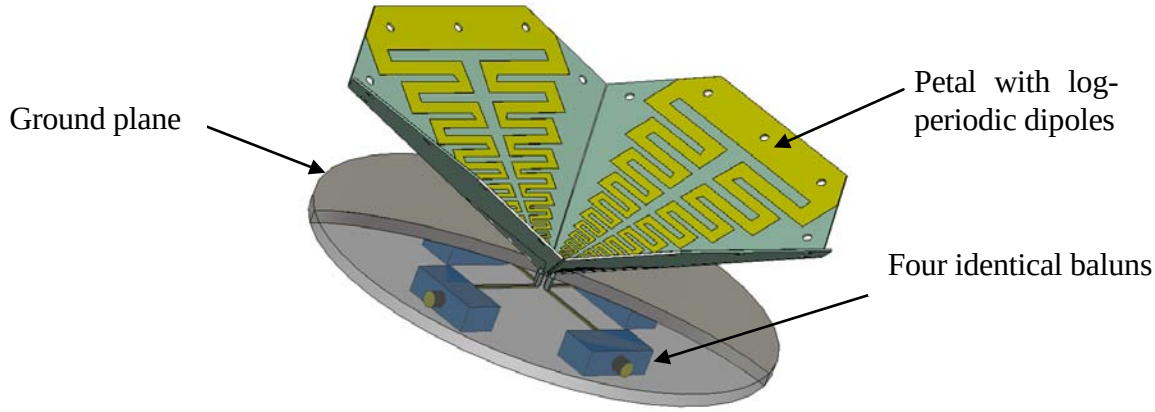

Figure 3.1: Eleven antenna with the baluns

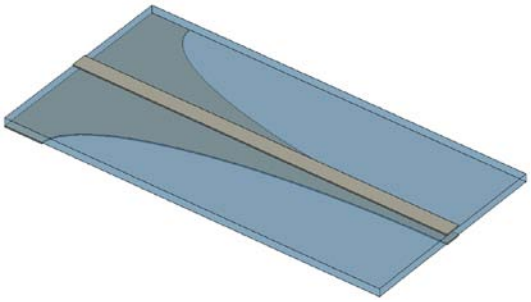

Figure 3.2: Simple microstrip to stripline balun.

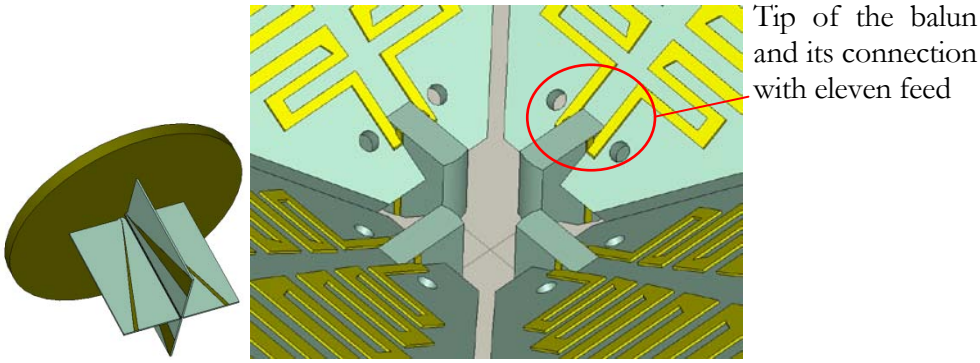

Figure 3.3: Arrangement of four baluns behind the ground plane for two polarization and connection with the Eleven feed.

In literature, there is another terminology describing the balance quality is 'balun ratio' [48] or BR. It is define as the ratio of the current exciting desired balance mode to the current exciting undesired unbalance mode. In term of S-parameters, the balun ratio is $(S_{31} + S_{21})/(S_{31} - S_{21})$.

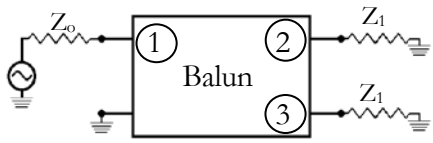

Figure 3.4: Block diagram of a typical balun.

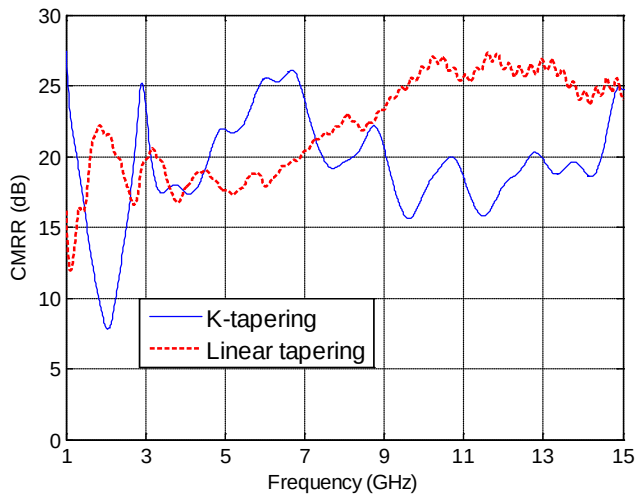

Figure 3.5: Simulated CMRR of the two baluns.

3.1 Design and Integration

Since a balun can be consider as a matching network for transforming the high impedance balanced load to an unbalanced load. For Eleven feed the differential impedance is very high which require a broadband matching technique. Two versions of the Eleven feed have been made with two different balun designs. The first version of balun was designed using optimization technique available in CST Microwave Studio, which we called 'Linear Tapering'. This design doesn't provide the satisfactory reflection coefficient. In the second version, the tapering of the balun has been done using Klopfenstein technique, which is a method for broad band matching. Figure 3.5 shows the simulated CMRR, calculated using CST Microwave Studio, of the two versions which is about 17 dB over the desire bandwidth. Balun with linear tapering seems have lower CMRR at about 2 GHz. One method for confirming the performance of the balun is to connect it in the back–to–back configuration at their balanced ports, see Figure 3.6. Simulated and measured reflection and transmission coefficients are shown in Figure 3.7. The reflection coefficient is below -10 dB for 2.5 – 16 GHz, which means that a

single balun should have below - 12 dB performance. The measured transmission coefficient agrees well with the simulated one, except for some dips at a few frequency points. This may be caused by some resonances within the metal support frame.

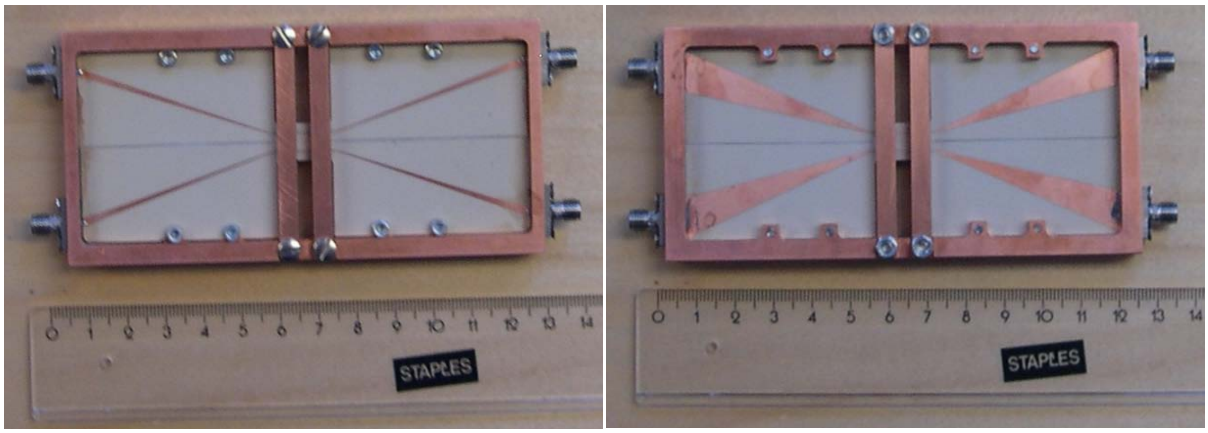

Figure 3.6: Tapered microstrip balun with back-to-back configuration.

Detailed design of linear tapering balun is shown in Figure 3.8. Each twin balun board is 50 mm wide and 50.87mm long. Optimization has been done on the criteria of length and tapering of the balun. Substrate material used in the balun is the same as used for the petal of Eleven feed, i.e. 0.762 mm thick Rogers TMM3. The baluns are then shielded with a metallic box. The metallic box is also partitioned diagonally, so as to reduce the coupling between the baluns. The cavity resonances introduced by the shielded metallic box can be suppress by using 1 mm thick Eccosorb MCS absorbing sheet, which is placed on the inner side of the shielded metal box. This balun transform the 200 ohm differential impedance of the Eleven feed to single ended 50 ohm. This can easily be achieved by gradually decreasing the width of both upper and lower conductors of the balun.

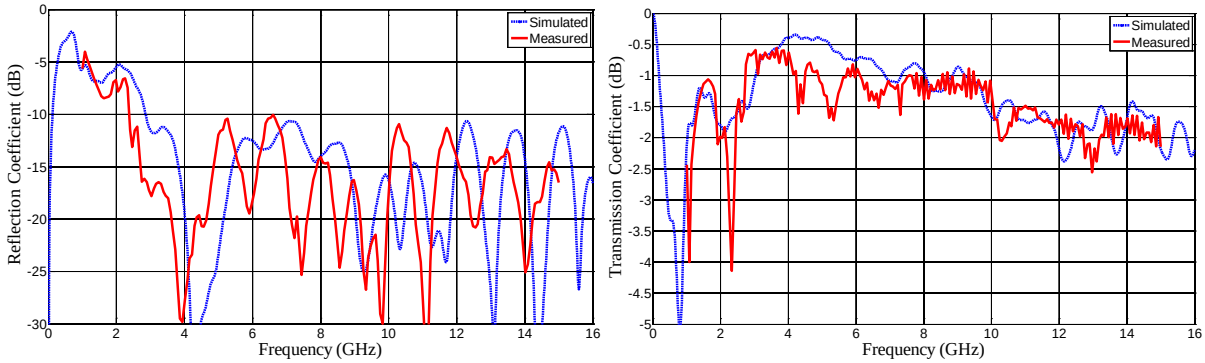

Figure 3.7: Simulated and Measured S-parameters of back-to-back balun.

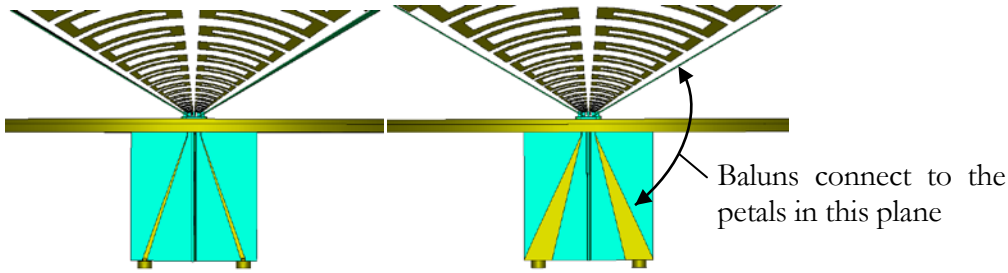

Figure 3.8: Geometry of the version 1 twin tapered microstrip line balun shows the front (left) and rear (right) sides of the circuit board.

Version 2 of the balun is based on Klopfenstein tapering technique, which we called K-Tapering. Other changes are that the differential impedance of the Eleven feed is set to have value of 250 ohm. For this high impedance matching, the substrate material has been changed to 0.787 mm thick Rogers 5880. Similarly the size of the board is now increased to 110 x 71.25 [mm^2], which is twice wider than the linear tapering balun, see Figure 3.9.

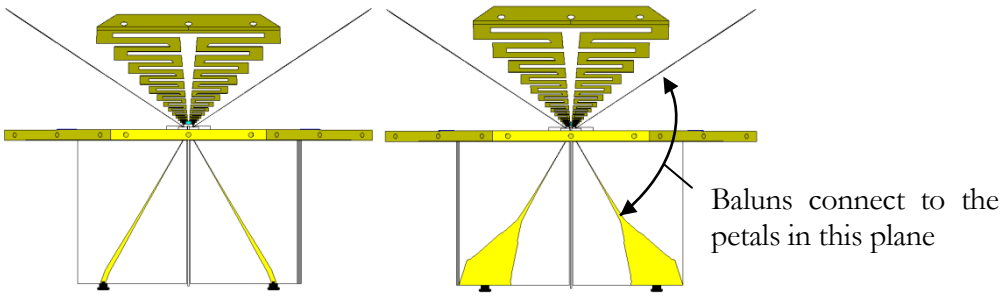

Figure 3.9: Geometry of the version 2 twin tapered microstrip line balun shows the front (left) and rear (right) sides of the circuit board.

3.2 Measurement Setup and Results

The two versions of the balun have been manufactured and the performance of the Eleven feed have also been measured both in anechoic chamber and in the reverberation chamber [49]. Figure 3.10 shows the two prototypes of the Eleven feed together with a compact low-loss decade-bandwidth power combiner using Gap-waveguide technology [50]. The power combiner has a size of 31.58×15.79×7.9 mm^3 and a reflection coefficient below -12 dB over 2-14 GHz. The dimensions of the Eleven feed remain same in both cases. The balun with linear tapering is shown in left side of Figure 3.10, whereas balun with Klopfenstein tapering technique is shown in the middle. The actual performance of the balun is measured by connecting it with the Eleven feed and enclosing it in a metallic box. With the enclosure in a metallic box, the characteristic impedance of the balun lines

changes as well as the common mode start to propagate along the line. This will affect the BOR_1 efficiency [51]-[54]. Numerical studies show that the CMRR of both the baluns are around 17 dB in the desired bandwidth. This also includes the affect of ground plane of the Eleven feed as the balance lines are passing through the holes in the ground plane and this cannot be avoided. Similarly the cavity resonance, which might be excited due to the metallic box, can be suppressed by absorbing sheet.

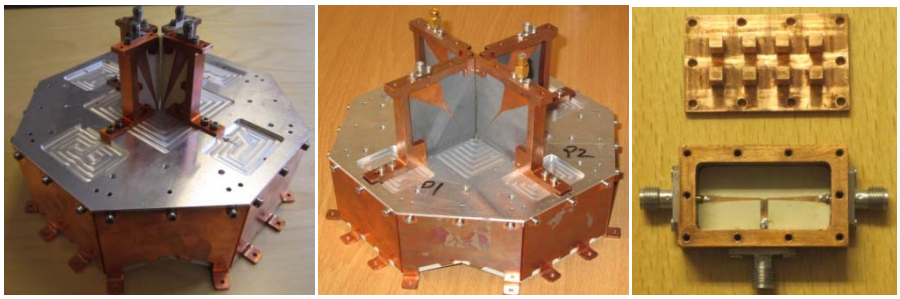

Figure 3.10: Two versions of the Eleven feed with balun, linear tapering balun (Left) and K-tapering balun (middle). The power combiner (right) is used to combine the two output ports of each polarization. All measurements with the Eleven feed include the power combiner.

Figure 3.11 shows the reflection coefficient of the Eleven feed with balun (four linear tapering baluns and two wideband power combiners). The result shows that S_{11} is below -8 dB except few frequency points. This is measured by properly terminating the ports of the baluns of other polarization. It should be noted that the mechanical tolerance has an effect on the reflection coefficient performance of the feed, especially the contact point where the balance twin line connect to the antenna terminal, see Figure 3.3 again.

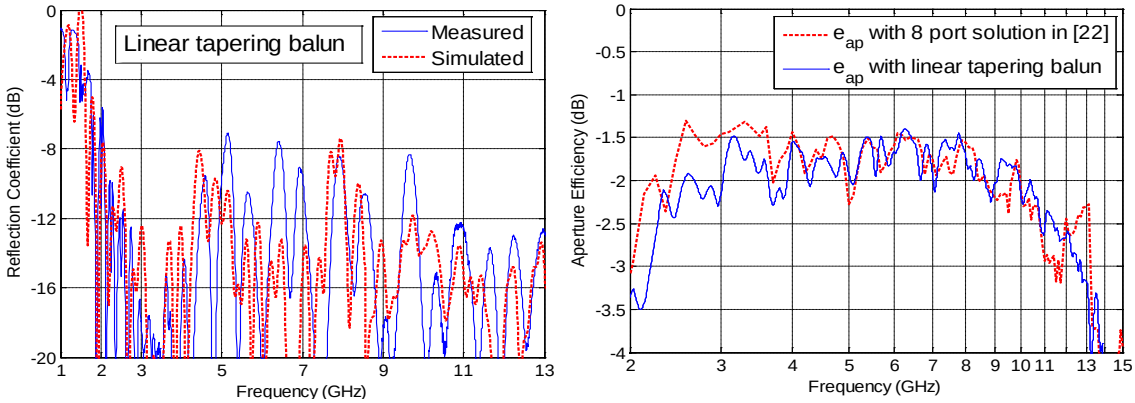

Figure 3.11: Measured reflection coefficient (left) and Efficiency of the feed (right) with balun feeding.

The radiation patterns of the Eleven feed at various frequencies have been measured and they are satisfying the property of constant radiation characteristics of Eleven antenna as stated in [22], over the whole 2 - 14 GHz bandwidth. The total aperture efficiency and its sub – efficiencies as defined in [51] and [52] are calculated based on radiation patterns measurement. In order to assess the performance of the baluns with the Eleven feed, we compare the aperture efficiency e_{ap} of the Eleven feed with the baluns to that with 8-port solution in [22]. Note that the feed illuminates a symmetrical paraboloid with a subtended angle of 2×60° and the center blockage loss is neglected in the e_{ap} calculation. From Figure 3.11, we see that the aperture efficiency of the feed with the linear tapering balun feeding follows that with the 8-port feeding, with 0.5 dB lower from 2 to 14 GHz.

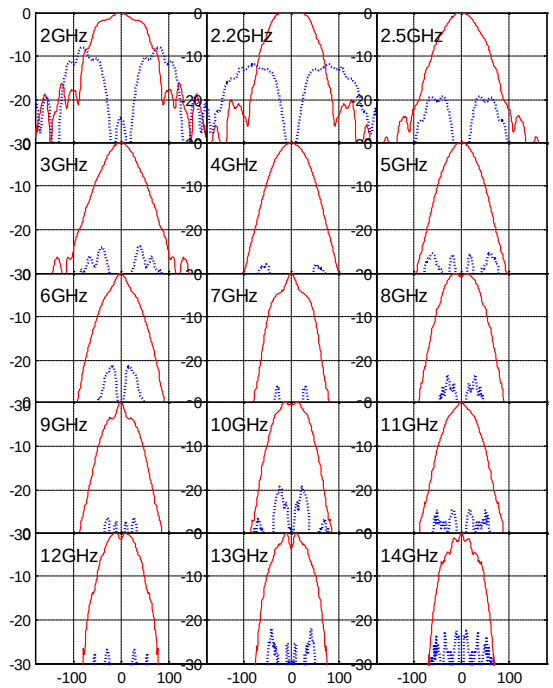

Figure 3.12: Measured co – and cross – polar BOR_1 radiation patterns in φ = 45 plane.

Figure 3.12 shows the measured co and cross – polar radiation patterns of the BOR_1 components in the φ = 45° plane. BOR_1 pattern are measured by the method describe in [54].

The second prototype of the K-tapering balun feeding has been made in order to improve the reflection coefficient. Broadband matching techniques were used to improve the matching between the balance port and antenna terminal. Figure 3.13 shows the measured reflection coefficient of the Eleven feed with balun of K-tapering. The result shows that S_{11} is now improved and below -10 dB

except for few frequency points where it goes up to -8 dB at around 5 GHz and between 8 – 9.5 GHz, and these are small peaks. Similarly the aperture efficiency, along with BOR_1 efficiency is shown in Figure 3.13. By definition, BOR_1 efficiency is a measure of the power lost in higher order azimuth variations of the far field of the antenna. These variations represent losses, and they can never contribute to the directivity, in fact they contribute to the side lobes [54]. The aperture efficiency follows that with the 8-port feeding up to 8 GHz (0.5 dB lower from 1 GHz to 4 GHz), then however degraded between 8-9.5 GHz. From 10 to 15 GHz, the aperture efficiency of the K-tapering balun feeding is much better than that of the 8-port solution: 1–1.5dB improvement up to 15 GHz. The reason that the e_{ap} for the K-tapering balun feeding is degraded between 8–9.5 GHz, we believe, is that the CMRR performance of the K-tapering balun does not have very robust immunity to strong reflection at the interface between the balun and the Eleven feed, which we did not consider when we designed the balun separately. As it is shown in Figure 3.13, there is a strong reflection (about -8 dB) between the balun and the feed for the K-tapering feeding. This reflection excites common modes which then cause the BOR_1 efficiency (a measure of how symmetric the radiation pattern is) degrading, as shown in Figure 3.13. This phenomenon leads to low aperture efficiency. As a contrast, the linear tapering balun has better immunity to strong reflection, where though the reflection coefficient is high (a bit above -8 dB), the e_{ap} is not degraded. However, the performance of reflection coefficient and aperture efficiency at high frequency end of the linear tapering balun is inferior to that of the K-tapering balun. A study is now being carried out to solve this problem of the BOR_1 efficiency drop between 8 – 9 GHz.

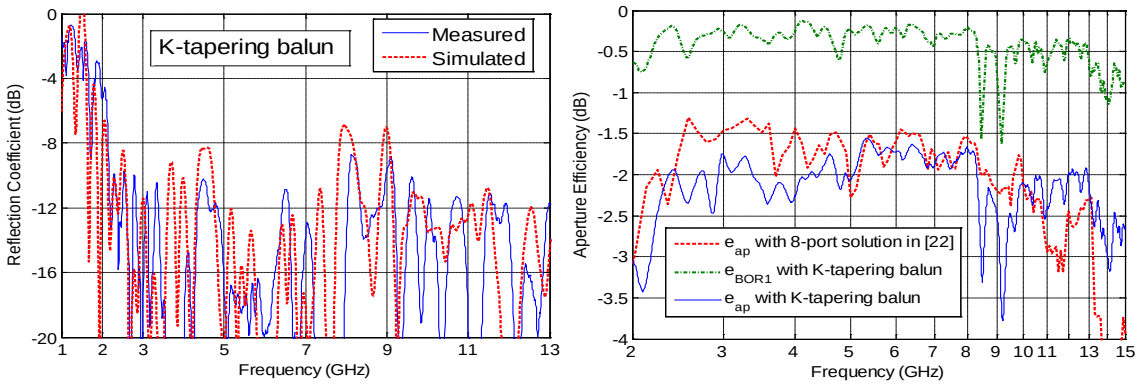

Figure 3.13: Measured reflection coefficient (left) and Efficiencies of the feed with balun feeding (right).

Figure 3.14 shows the measured co and cross – polar radiation patterns of the BOR_1 components in the $\varphi = 45^o$ plane. It can be seen that the radiation pattern is not the same as that in the case of linear tapering at 9 GHz.

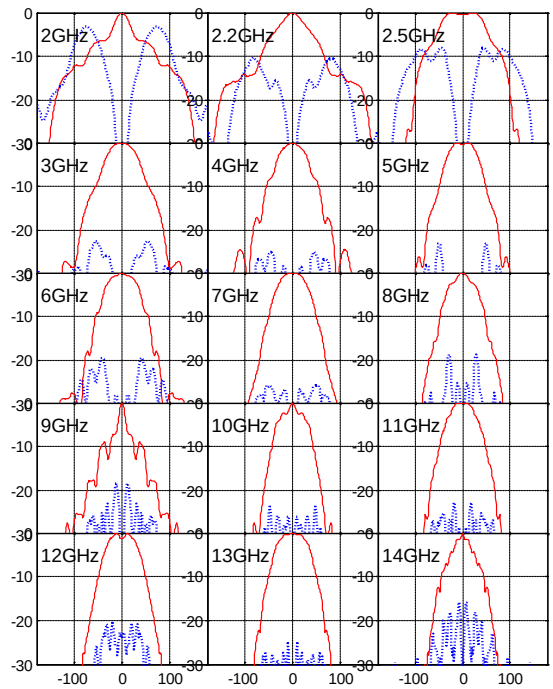

Figure 3.14: Measured co – and cross – polar BOR_1 radiation patterns in $\varphi = 45$ plane.

3.3 Measurement of Radiation Efficiency of Multiport Antennas

It is often required, particularly for integrated antenna systems in radio telescopes, that the radiation efficiency of a multiport antenna, excluding the losses in the feeding network, should be measured before being integrated in the system. The radiation efficiency of a multiport antenna e_{rad_ANT} consists of two factors: the ohmic losses in the antenna itself and the so-called decoupling efficiency that accounts for power returned to non-excited ports, as defined in [55] (Note that e_{rad_ANT} here corresponds to ε_{totrad} in [55]). Both factors depend on the excitations provided by feeding networks. However, the test feeding network is often built up of commercially available components in order to reduce the development cost. The losses in the test feeding network could be large, and the impedance match between the antenna and the test feeding network could be far from the perfect case. Thus, it is not a trivial task to obtain the radiation efficiency of a multiport antenna excluding the losses in feeding network. A rigorous feeding network correction approach for obtaining the radiation efficiency of a multiport antenna has been presented. This method uses measurement data of the total

radiation efficiency of a multiport antenna with a multiport feeding network, the S-matrices of the feeding network and the antenna, to calibrate out the losses in the feeding network.

Figure 3.15 shows the block diagram of a general multiport antenna with a multiport feeding network. By multiport antenna, we refer it to the multiport antenna without feeding network. The total radiation efficiency of the whole antenna system with the feeding network e_{tot_ANTFN} is defined as

$$e_{tot_ANTFN} = \frac{P_{rad}}{|a_1|^2} \tag{1}$$

where P_{rad} is the total radiated power from the antenna and $|a_1|^2$ is the input power.

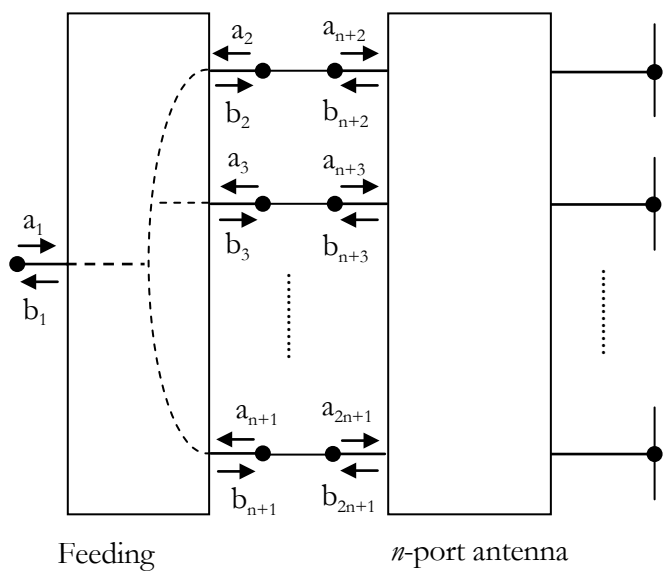

Figure 3.15: Block diagram of the configuration of an n-port antenna with its feeding network.

The radiation efficiency e_{rad_ANT} of the multiport antenna can be expressed as

$$e_{rad_ANT} = \frac{P_{rad}}{\sum_{k=n+2}^{2n+1}(|a_k|^2 - |b_k|^2)} \tag{2}$$

which measures both the ohmic losses and the decoupling efficiency to non-excited ports in the multiport antenna. The multiport feeding network can be expressed by the following S-matrix

$$\begin{bmatrix} \boldsymbol{b}_I \\ \boldsymbol{b}_{II} \end{bmatrix} = \begin{bmatrix} \boldsymbol{S}_{I,I} & \boldsymbol{S}_{I,II} \\ \boldsymbol{S}_{II,I} & \boldsymbol{S}_{II,II} \end{bmatrix} \begin{bmatrix} \boldsymbol{a}_I \\ \boldsymbol{a}_{II} \end{bmatrix} \tag{3}$$

where

$$\boldsymbol{b}_I = [b_1], \qquad \boldsymbol{a}_I = [a_1], \qquad \boldsymbol{b}_{II} = \begin{bmatrix} b_2 \\ \vdots \\ b_{n+1} \end{bmatrix}, \qquad \boldsymbol{a}_{II} = \begin{bmatrix} a_2 \\ \vdots \\ a_{n+1} \end{bmatrix}$$

$$\boldsymbol{S}_{I,I} = [S_{11}], \qquad \boldsymbol{S}_{I,II} = [S_{12} \quad \cdots \quad S_{1,n+1}]$$

$$\boldsymbol{S}_{II,I} = \begin{bmatrix} S_{21} \\ \vdots \\ S_{n+1,1} \end{bmatrix}, \qquad \boldsymbol{S}_{II,II} = \begin{bmatrix} S_{22} & \cdots & S_{2,n+1} \\ \vdots & \ddots & \vdots \\ S_{n+1,2} & \cdots & S_{n+1,n+1} \end{bmatrix}$$

where S_{ij} is the S parameter of the feeding network from port j to port i. Similarly, the multiport antenna can also be expressed by an S-matrix as

$$\boldsymbol{b}_{III} = \boldsymbol{S}_{III}\boldsymbol{a}_{III} \tag{4}$$

where

$$\boldsymbol{b}_{III} = \begin{bmatrix} b_{n+2} \\ \vdots \\ b_{2n+1} \end{bmatrix}, \qquad \boldsymbol{a}_{III} = \begin{bmatrix} a_{n+2} \\ \vdots \\ a_{2n+1} \end{bmatrix}, \quad \boldsymbol{S}_{III} = \begin{bmatrix} S_{n+2,n+2} & \cdots & S_{n+2,2n+1} \\ \vdots & \ddots & \vdots \\ S_{2n+1,n+2} & \cdots & S_{2n+1,2n+1} \end{bmatrix}$$

From Figure 3.15, we have,

$$\boldsymbol{a}_{II} = \boldsymbol{b}_{III}, \;\; \boldsymbol{b}_{II} = \boldsymbol{a}_{III} \tag{5}$$

Therefore, from (3), (4) and (5), we can obtain

$$\boldsymbol{a}_{III} = \left(I - \boldsymbol{S}_{II,II}\boldsymbol{S}_{III}\right)^{-1}\boldsymbol{S}_{II,I}\boldsymbol{a}_I \tag{6}$$

where I is the identity matrix. Therefore, e_{rad_ANT} can be expressed as

$$e_{rad_ANT} = \frac{P_{rad}}{|\boldsymbol{a}_{III}|^2 - |\boldsymbol{b}_{III}|^2}$$

$$= \frac{e_{tot_ANTFN}}{\left|\left(I - \boldsymbol{S}_{II,II}\boldsymbol{S}_{III}\right)^{-1}\boldsymbol{S}_{II,I}\right|^2 - \left|\boldsymbol{S}_{III}\left(I - \boldsymbol{S}_{II,II}\boldsymbol{S}_{III}\right)^{-1}\boldsymbol{S}_{II,I}\right|^2}. \quad (7)$$

Thus, the radiation efficiency e_{rad_ANT} of a multiport antenna can be calculated by measured data of the total radiation efficiency e_{tot_ANTFN}, and S-matrices of the feeding network and the multiport antenna. An approximate method was used in [22] to determine the radiation efficiency, where a perfect impedance matching was assumed between the antenna and the feeding network, i.e. $S_{III} = 0$, which leads from (7) to

$$e_{rad_ANT_approx} = \frac{e_{tot_ANTFN}}{\left|\boldsymbol{S}_{II,I}\right|^2} \quad (8)$$

The above expression corresponds to the case that the radiation efficiency of a multiport antenna is approximately equal to the total radiation efficiency of the antenna with the feeding network subtracted by the insertion loss of the feeding network.

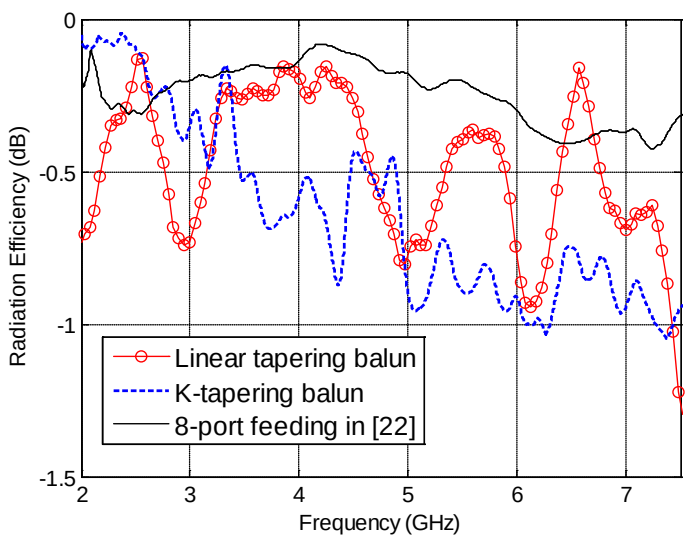

Figure 3.16: Radiation efficiency of the Eleven antenna obtained from the measurements.

Figure 3.16 shows the measured radiation efficiency by using the reverberation chamber technique over 2–8 GHz, which is the available operating frequency band of the chamber [49]. It is observed that

the radiation efficiency of the balun feedings, including baluns and power combiner, is less than -1 dB over 2–8 GHz, a very good performance. But it is still 0.5 dB more loss than that of the 8-port feeding solution in [22], which is a drawback for the passive balun solution.

Chapter 4

Dual Polarized Self-grounded Bowtie Antenna

The purpose of this work is to design such a dual-polarized self-grounded bowtie antenna that can be used in both MIMO systems and radar (or sensor) systems over an octave bandwidth, 1.5–3 GHz. The design is carried out by optimizing the geometry of four equal petals grounded to the same ground plane and located on the same side of it. The directivity of each petal of the bowtie antenna is similar to that of the theoretical Huygens source, which makes it an interesting antenna for achieving the best available MIMO coverage of small antennas.

4.1 Design and Geometry Optimization

The geometry of the self grounded bowtie antenna is shown in Figure 4. 1. The structure is based on the design presented in [39], [40]. The bowtie is placed over the ground plane, with arms making a certain angle θ. Then in the end, the bow is folded down to make a circular shape and connected with the ground plane, as shown in Figure 4. 1. Each bow is fed individually with a coaxial port matched to 50 ohm. The profile of the bowtie is modified to match it with the 50 ohm feed line. Figure 4. 1a, shows the variation in the bow-tie profile, compare to a normal triangular shaped petal.

First, the profile of triangular shaped bowtie antenna is modified in the planar 2D form. The hypotenuse of the triangle is made by sinusoidal analytical curve controlled by some variables defining the amplitude and its period. This will modify the shape of the bowtie as shown in Figure 4. 1a. Then this 2D planar shape bowtie is bended over a cylinder at the edge of the ground plane (later that cylinder will be removed), as shown in Figure 4. 1b. Only half the circumference of the cylinder used to bend the planar shape. The remaining part of the petal is planar, being tangential to the surface of the virtual cylinder. The narrowest part of the bow, which is now bended toward the center of the ground plane, then connected to a coaxial cable making an angle θ with the ground plane (see Figure 4. 1b and c). So, the design parameters, which describe this antenna, are the variables controlling the profile, the angle θ, the location and height ℓ of the central support block with the coaxial feed point, the width of the ground plane, and the radius of curvature of the bowed part of the petal, and the profile of the petals. In the center, to make the antenna more stable, all the feeding points are

supported by a substrate block made by Teflon. On the back side of the ground plane, four single ended coaxial ports will appear, see Figure 4. 1d, where the identical length, semi ridged coaxial cables can be bended on the same side and connected with female SMA connectors fastened to a metal frame that supports the ground plane (Figure 4. 1e). This arrangement will make it possible to use this self-grounded bowtie antenna either as a MIMO antenna with four single ended ports, or a directional antenna with two differential ports (e.g. for LoS antenna system or as a feed of a reflector antenna). To form the differential ports we will need two 180° hybrids or baluns.

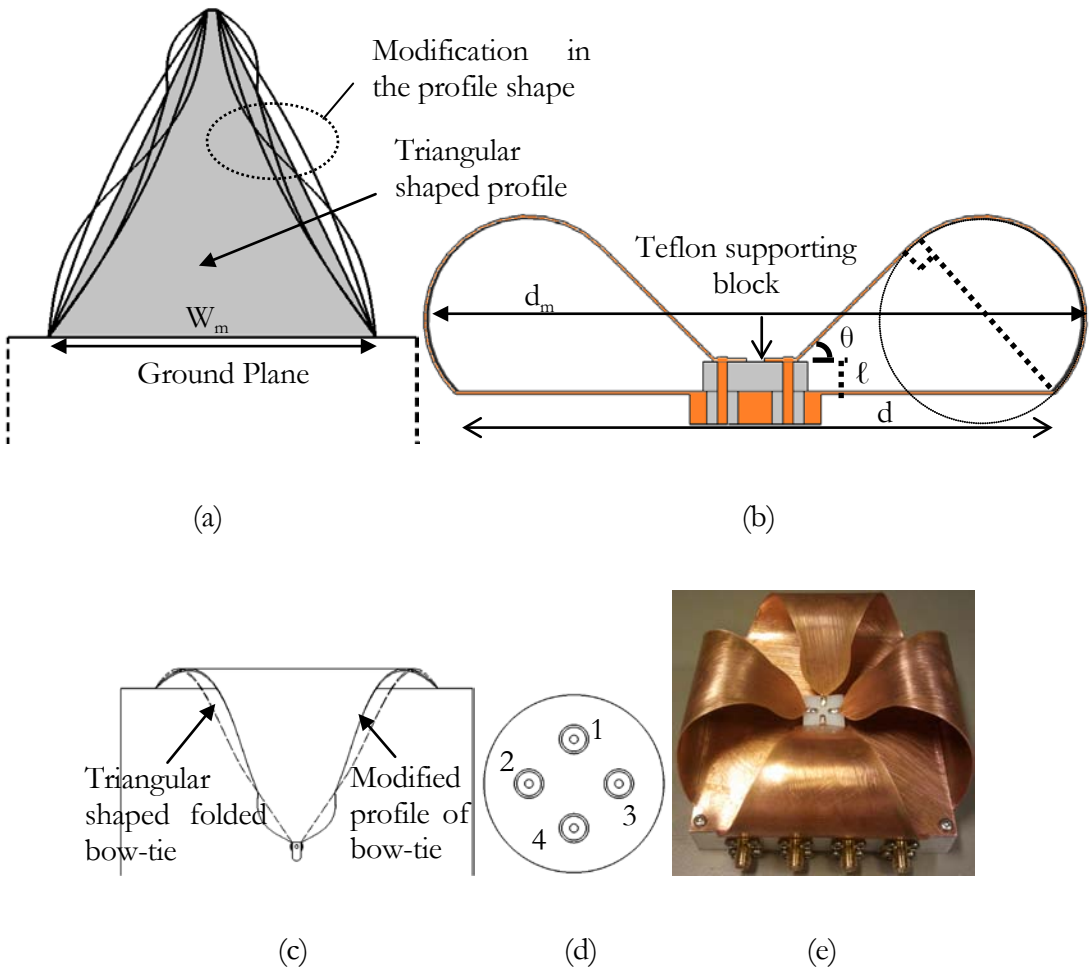

Figure 4. 1 Basic geometry of the self-grounded dual polarized bowtie antenna, a) Unfolded 2-D view of a petal, b) Cross-sectional view with important parameters, c) Top view of a folded single petal, d) the four numerical coaxial input ports on the back side of the ground plane, e) 3-D view of the integrated self-grounded bowtie antenna.

We used the optimizer available in CST Microwave Studio [56] to optimize the geometry of the antenna through the above defined parameters with the goal function as the differential reflection

coefficient should be below -15 dB between 1.7-2.9 GHz. This optimization criterion was chosen because we originally looked for a dual-polarized directive beam, and the differential excitation is the only one that can provide that.

4.2 Performance

As it is already stated previously that the bowtie antenna were design to have four 50 ohm coaxial ports on the back side of the ground plane. This will make it easy to mount the antenna on a post for different applications. A prototype of the dual polarized self-grounded bowtie antenna has been manufactured and measured, in order to verify the performance of the antenna according to the simulated results. Figure 4. 1e shows the photo of the manufactured antenna. Figure 4. 2 show the simulated as well as measured reflection coefficient for the cases of single port excitation and differential excitation. Single port excitation means that only one port is excited at a time and all other ports are terminated with 50 ohm loads. For differential port excitation, opposite ports are excited with the same amplitude and 180° phase difference, i.e. ports (1,-4) or (2,-3). It can be seen that the simulated S_{11} for single port excitation is below -10 dB between 1.5 – 2.7 GHz, whereas for differential excitation, -10 dB bandwidth is 1.6 – 3 GHz.

Figure 4. 3 show the radiation efficiencies for the cases of the single port excitation as well as differential port excitation. Similarly, the total radiation efficiency for single port is about -1.3 dB. This is because of the high reflection coefficient compare to differential port excitation and the decoupling loss to the other ports. The directivity of the self grounded bowtie antenna is shown in Figure 4. 4, which is about 4 – 6.5 dBi over the frequency band of 1.5 – 3 GHz.

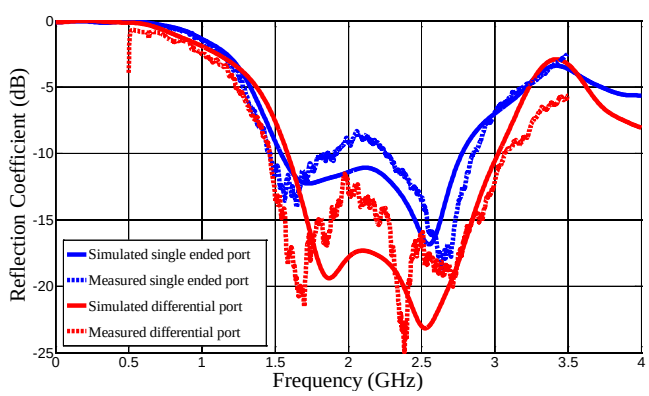

Figure 4. 2 Simulated and measured reflection coefficient.

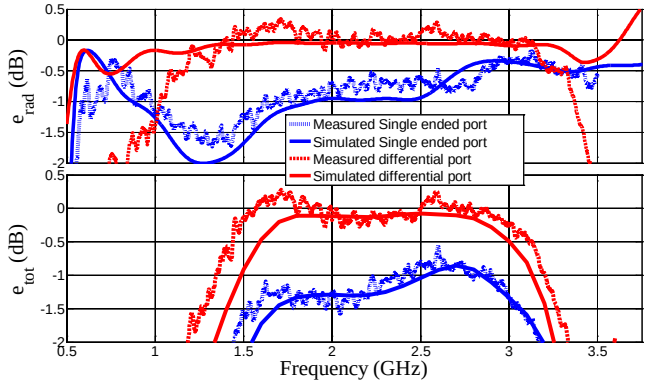

Figure 4. 3 Simulated and measured efficiencies of the Bowtie antenna, with single port and differential port configuration.

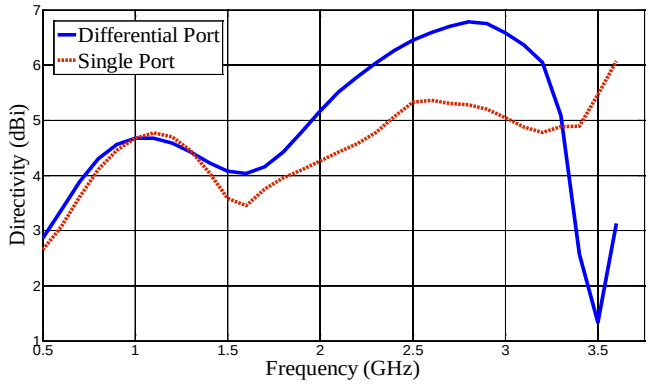

Figure 4. 4 Directivity of the bowtie antenna for differential excitation and single-port excitation.

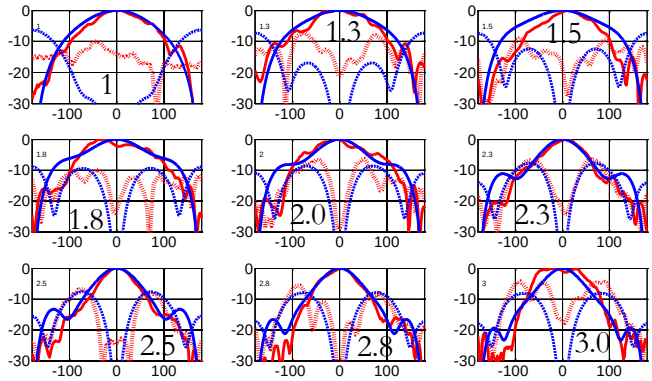

Figure 4. 5 Simulated and measured Co (solid line) and cross (dashed) polar radiation pattern at 45° plane.

The simulated and measured radiation patterns at 45° plane are shown in Figure 4. 5 at different frequencies (from 1-3 GHz). It looks that the radiation pattern is quite stable and directed normally to the ground plane of the bowtie antenna. Both simulation and measurement are quite good in agreement.

Chapter 5

Numerical ports and characteristic impedance of gap waveguide

In order to obtain the propagation characteristics of the gap waveguide, a numerical study on the similarity between the hollow (rectangular and ridge) waveguides and the gap (groove and ridge) waveguides has been carried out in term of dispersion diagram and characteristic impedance.

5.1 The Dispersion Diagram

The dispersion diagrams of the rectangular/ridge waveguides and the groove/ridge gap waveguides are simulated for the infinitely long periodic structures along the direction of propagation, shown in Figure 5. 1, using the Eigenmode solver in CST Microwave Studio [56]. The material used here in the simulation is perfect electric conductor with no surface roughness. Cross sectional views of the geometries with the dimensions used in the simulation are summarized in Table 5. 1 , where the dimensions are chosen in agreement with those in [30] in order to obtain a targeted stopband from 10 to 20 GHz. Note that the width and the periodicity of the pins play significant roles to determine the stopband [30].

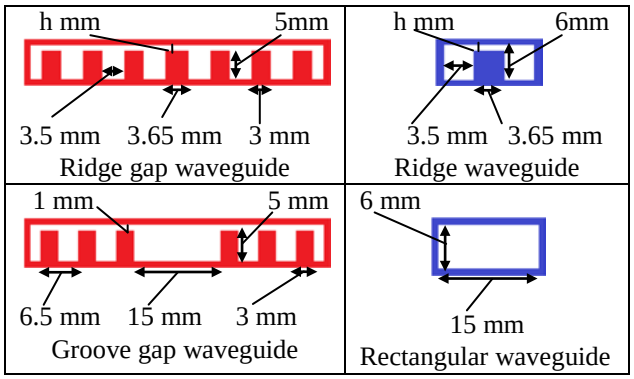

Table 5. 1 Cross-sections with dimensions of the simulated ridge and groove gap waveguides (left), and of the equivalent hollow ridge and rectangular waveguides (right).

The simulated dispersion diagrams of the ridge gap waveguide and classical hollow ridge waveguide are shown in Figure 5. 1 for four different gap heights above the ridge, i.e. h = 0.5 mm, 1 mm, 2 mm and

3 mm. The pin heights and the air gap above pins remain the same for all cases. We see that the stopband of the parallel-plate modes for these specific cases is between 11 and 22 GHz. The fundamental mode of the ridge gap waveguide is seen to have a dispersion curve that is very close to the light line (TEM mode) if the gap is kept small, as expected. However, it moves away from the light line when the gap between the ridge and the top metal plate is increased. Nevertheless, the dispersion curves of the ridge gap waveguide are very close to the fundamental mode curves of the equivalent hollow waveguides within the stopband of the parallel-plate modes. Similarly we have in Figure 5. 2 compared the dispersion diagrams for the case of groove gap waveguide and normal rectangular waveguide. The groove gap waveguide has exactly the same height as that of the rectangular waveguide, i.e. 6 mm. The stopband for this specific groove gap waveguide is between 11 and 19 GHz. The fundamental mode propagating for both type of waveguides are almost similar within the stopband.

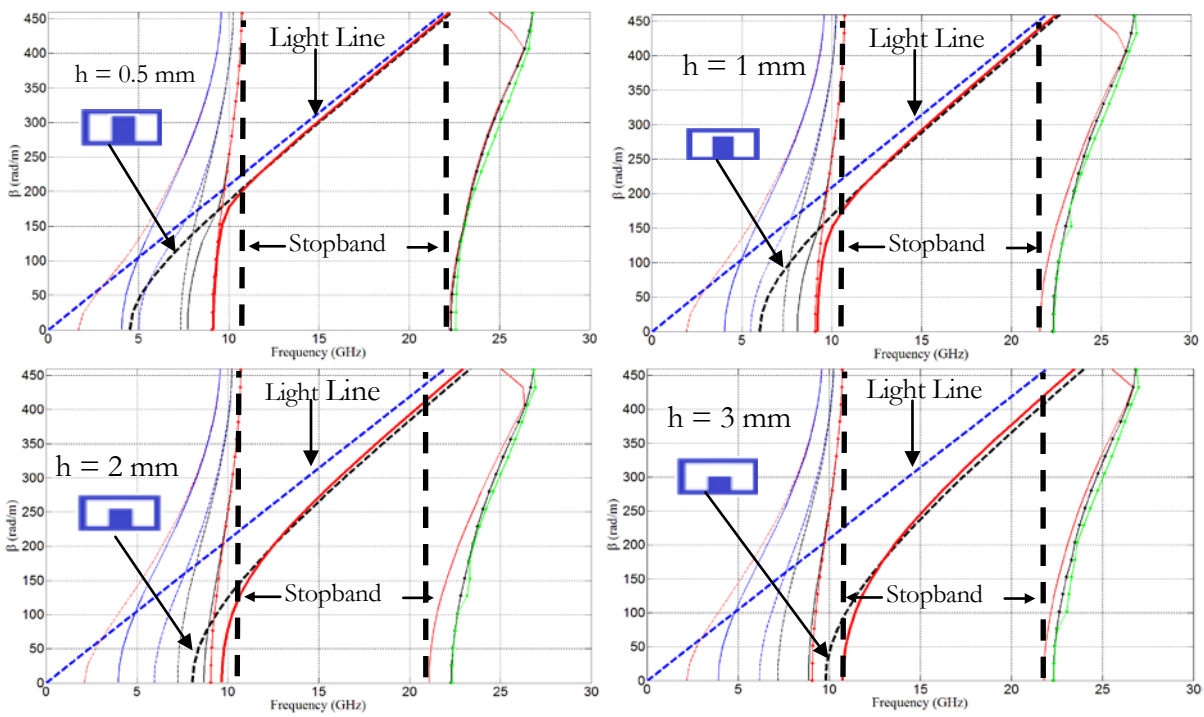

Figure 5. 1 Dispersion diagram of ridge gap waveguide with different gaps heights above the ridge. The pins and air gaps are the same for all cases. The two black vertical lines mark the beginning and end of the stopband, and the dashed solid line is the dispersion diagram of the equivalent hollow ridge waveguide

5.2 Direct Transition Between Hollow Waveguide and Gap Waveguide

The simulations in the present section have been done by using both CST and HFSS, two of the most used commercial electromagnetic solvers, on ridge/groove gap waveguides, with the dimensions shown in Table 5. 1and a length of 91.5 mm (See Figure 5. 3). We can easily observe that the results both by CST and HFSS are very similar, see Figure 5. 4.

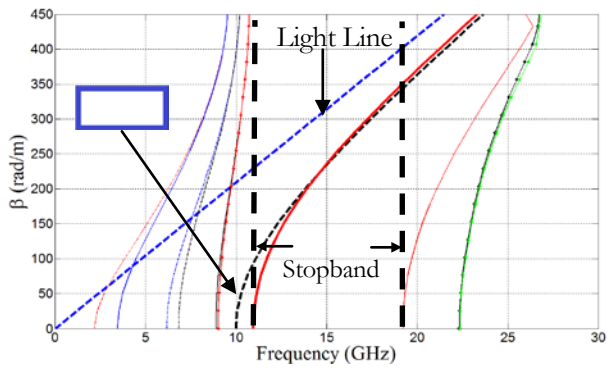

Figure 5. 2 Dispersion diagrams of groove gap waveguide and equivalent rectangular waveguide (dashed black line). The two black vertical lines mark the beginning and end of the stopband

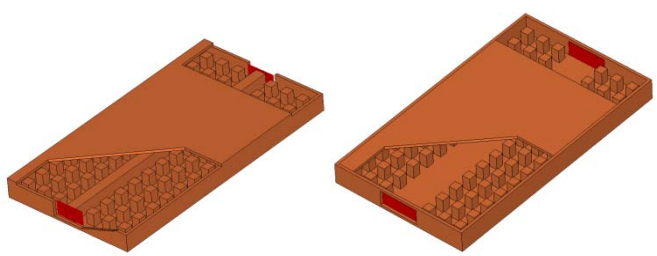

Figure 5. 3 Port configuration for simulating the S-parameters of the gap waveguides.

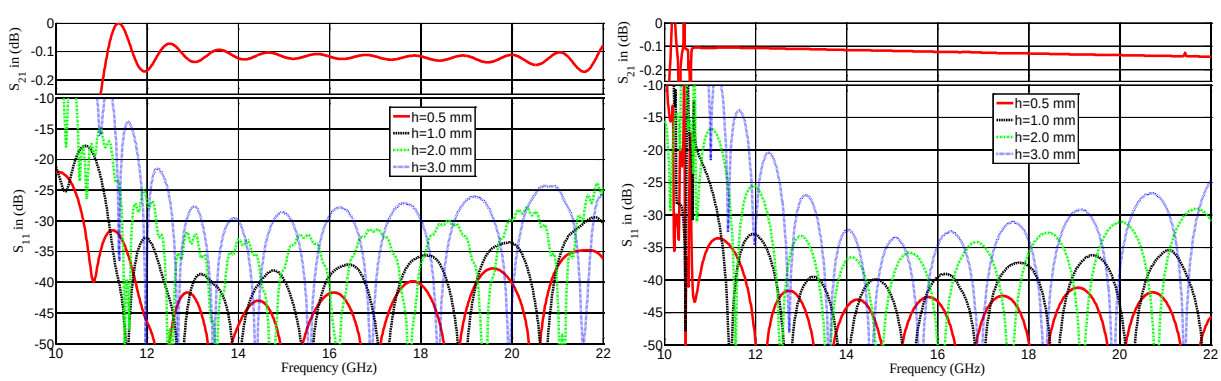

Figure 5. 4 S-parameters of the waveguide for the gap, using CST (left) and HFSS (right)

The numerical waveguide ports are defined to attach with the equivalent hollow waveguides with the same dimensions as the gap waveguides, shown in Figure 5. 3. We have also done simulations on both gap waveguides by making ridge waveguide interface on both sides of ridge gap waveguide as well as rectangular waveguide interface on both sides of groove waveguide. These arrangements also produce similar S-parameters as in the case shown in Figure 5. 4, where the numerical ports are directly attached to the gap waveguides. Figure 5. 4 and Figure 5. 5 show the S-parameters for the two cases, i.e., ridge gap waveguide and groove gap waveguide, respectively. The dimensions of the ridge gap waveguides are the same as the structure used for the dispersions diagrams in Figure 5. 1. We see that the reflection coefficients S_{11} of the ridge gap waveguide is below –35 dB if the gap above the ridge is smaller than or equal to 1 mm, whereas it increases when the gap increases. As predicted in all the dispersion diagrams, the stopband start from 11 GHz. Similarly, for the groove gap waveguide S_{11} is below -30 dB over most of the parallel-plate stopband, except in the beginning of it. Thus, the equivalence between the gap and hollow waveguide structures is good except near the beginning of the stopband. The periodic nature of the reflection coefficient comes from the two interfering reflections, from the port at each of the two ends of the waveguides. This means that each waveguide transition has a reflection coefficient that is 6 dB lower than the peaks of the combined reflection coefficient S_{11} [57]. The simulations have been done with copper as material which explains that the transmission coefficient S_{21} is about -0.2 dB within the part of the stopband where the reflection coefficient is low.

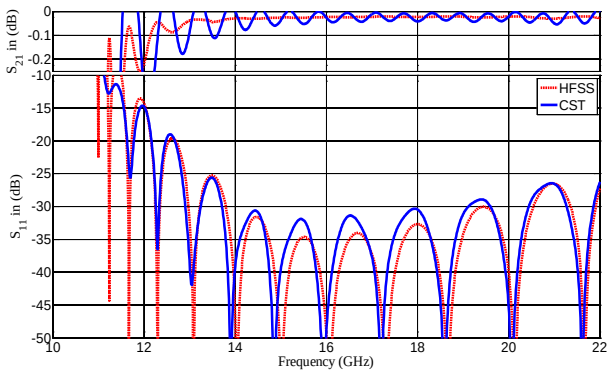

Figure 5. 5 S-parameters of the groove gap waveguide using CST and HFSS.

5.3 Characteristic Impedance of Ridge Gap Waveguide

The characteristic impedance of the ridge gap waveguide depends mainly on the width of the ridge and the air gap [58]. There are some methods available to calculate the approximate value of the characteristic impedance of ridge gap waveguide [59], [60]. We have already found that the reflection

coefficients compared to a numerical hollow waveguide flange is -30 dB. This indicates that the ports are well matched to the gap waveguides, and we can use, as a first approximation, the simulated characteristic impedance provided by the numerical field simulator for the equivalent hollow waveguide cases. Then, we apply a correction to the first-order approximated characteristic impedance by using the simulated reflection coefficient of the two-port network shown in Figure 5. 3, the gap waveguide under test with its equivalent waveguide ports at the two ends. The reflection coefficient **r** of one such transition is given by

$$\mathrm{r} = \frac{Z_o - Z_{port}}{Z_o + Z_{port}}; \quad Z_o = Z_{port}\frac{1+\mathrm{r}}{1-\mathrm{r}}$$

where Z_{port} is the characteristic impedance of the equivalent ridge waveguide, and Z_o is the characteristic impedance of the gap waveguide. The waveguide port impedances are provided both in CST and in HFSS over the whole frequency range. The S-parameter S_{11} of the two-port network in Figure 5. 3 can be estimated by using theory of small reflections in [57],

$$S_{11} \approx \mathrm{r}\left(1 - e^{-j2\beta l}\right)$$

where 'l' is the length of ridge waveguide. The absolute value of **r** will exactly be half of the magnitude of S_{11} at the peak values. This approximation is valid for small reflections, typical $|\mathbf{r}| < 0.2$. The above two equations enable us to calculate the characteristic impedance of the gap waveguides from the simulated S_{11} and the port impedances available from HFSS. With the values of the characteristic impedance at the peaks of S_{11}, the whole impedance curves can be interpolated and are shown in Figure 5. 6 for ridge gap waveguide of different air gap heights. The width of the ridge is kept the same in all cases.

The characteristic impedance for the case when the air gap above the ridge is 0.5 mm is exactly the same as that of the port impedance over the whole frequency band gap. This is because the reflection coefficient is below -40 dB for this case. Slight variations appear as the air gap increase to 1 mm and more. Again referring back to Figure 5. 1, it can be observed that within the stopband, the fundamental modes of both the ridge waveguide and ridge gap waveguide are exactly the same for the gap equal to 0.5 mm and 1 mm. However, for the gap equal to 2 mm and 3 mm, they are slightly different both at the beginning and at the end of the stopband. This might be the possible reason of

the impedance variation shown in Figure 5. 6 when the gap above the ridge is 2 mm and 3mm. The same procedure was adopted for the case of groove gap waveguide, where the wave impedance for the waveguide has been calculated through the port impedances. The results are shown in Figure 5. 7.

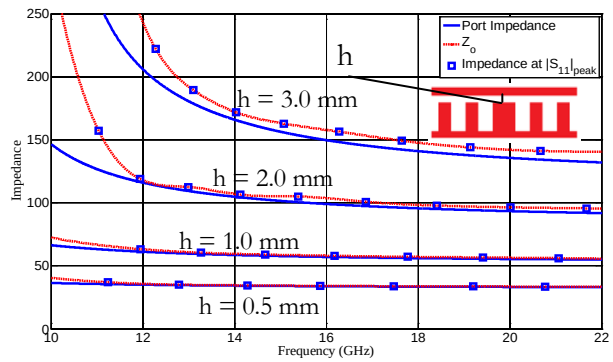

Figure 5. 6 Characteristic impedance of ridge gap waveguide from HFSS port model and our corrected result (Z_0).

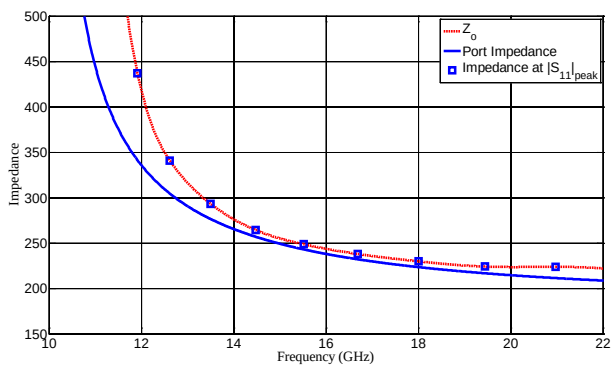

Figure 5. 7 Wave impedance in groove gap waveguide from HFSS port model and our corrected result (Z_0).

5.4 Pin Effect on Gap waveguide Microstrip Line

The geometry of the gap waveguide microstrip line is shown in Figure 5. 8. The periodic pattern of pins under the substrate material creates a PMC layer that forces the waves to propagate only in the narrow gap between the top metal plate and the metal above the substrate material, in the form of a quasi-TEM mode. Figure 5. 9 shows the S-parameters for the four cases: microstrip line above the pins, at the edge of pins, in between two pins and inverted microstrip line with ideal PMC boundary underneath. It can be seen that the reflection coefficients S_{11} of the straight gap waveguide microstrip line is different for each case. This clearly shows that there is a significant effect of the pins and their location relative to the microstrip line, especially at higher frequencies in the stopband. Several

methods have been analyzed to minimize the pin effect on the gap waveguide microstrip line. Among them is to make the microstrip line follows 45° to the pin pattern as shown in Figure 5. 10a. The reflection coefficients for each strip location relative to pins are shown in Figure 5. 10b. Although the variations in S_{11} still persist but it can be seen that the reflection coefficient is bellow -20 dB in each case for 45° orientation.

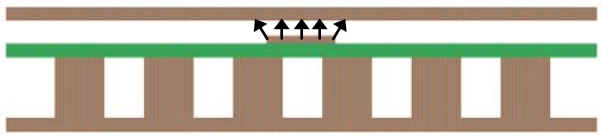

Figure 5. 8 Basic configuration of gap waveguide microstrip line. Grey color represents metal, and green color the substrate. The arrows indicate the field lines of the quasi-TEM mode.

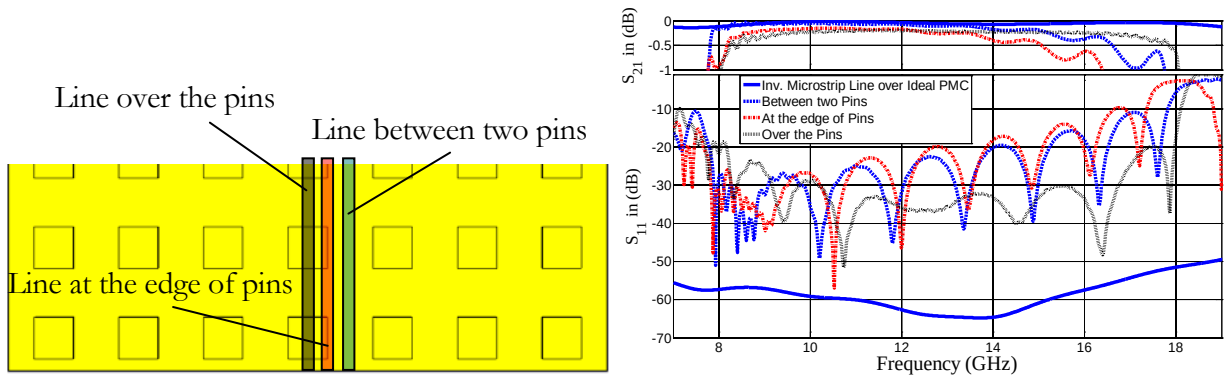

(a) (b)

Figure 5. 9 a) Position of gap waveguide line over the grid of pins. b) S-parameters of the waveguide for different locations of the microstrip line relative to the pin rows.

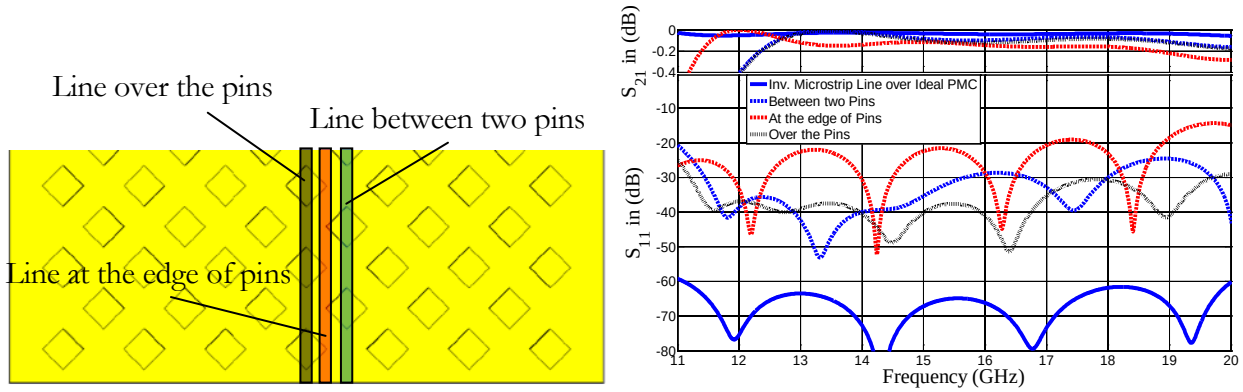

(a) (b)

Figure 5. 10 a) Position (relative to the 1st row of pins) of gap waveguide line over the 45° grid of pins. b) S-parameters for different locations of the microstrip line relative to the pin rows.

5.5 A Low Loss Rat Race Balun in Gap Waveguide Technology

Hybrid 3dB coupler (0° /180°) is often needed in feeding networks for antennas [61]. However, for high frequency applications, such as in millimetre wave, sub-millimetre wave and up to terahertz, it is very challenging to realize a low-loss and low-cost hybrid. Therefore, a prototype at 16 GHz is designed and manufactured. Simulations and measurements for this prototype are presented for the verification of the design. The geometry of the new hybrid is a gap-waveguide ring surrounded by metal pins which provide the parallel-plate stop band; see Figure 5. 11. In this work, the operating frequency band of 15-18 GHz has been chosen.

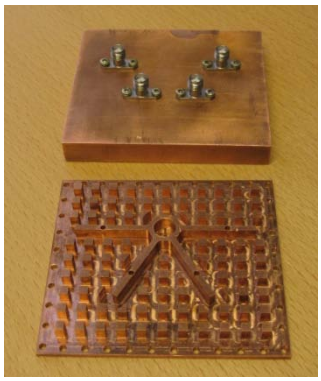

Figure 5. 11 Photo of the 15 – 17.5 GHz 3dB hybrid in ridge gap waveguide. The texture plate showing the ring hybrid surrounded by metal pins.

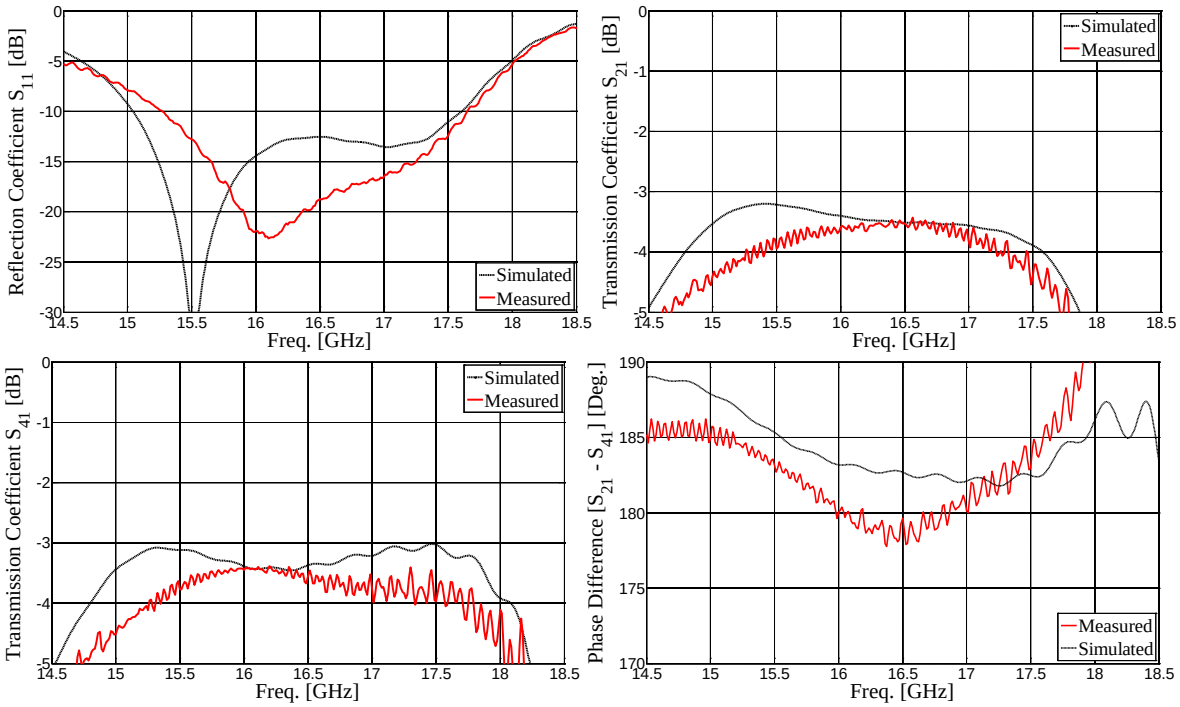

Figure 5. 12 Simulated & Measured S-parameters and phase difference of port 2 and port 4, when port 1 is input port.

Figure 5. 12 shows the simulated and measured reflection and transmission coefficients, respectively, when port 1 is the input port. It can be observed that the gap-waveguide ring hybrid has a very promising performance over the band of 15.25 – 17.75 GHz: the reflection coefficient is below -10 dB; the ohmic loss is very low, the transmission loss is mainly due to the mismatch loss; and the phase difference between the two output ports 2 and 4 is about 180° ± 5° as shown in Figure 5. 12. Similarly, Figure 5. 13 show the simulated and measured reflection and transmission coefficients, respectively, by considering port 3 as the input port, obtained by using CST MS. Again, it can be observed that the gap waveguide ring hybrid has a very promising performance over the band of 15.25 – 17.75 GHz. The measurement results follow the simulation results quite well in all figures. The reflection coefficient is below -10 dB; the ohmic loss seems very low; and the phase difference between the two output ports 2 and 4 is about ± 5°. An empirical formula for design of the 3dB hybrid by gap waveguide was introduced in [62] after this work.

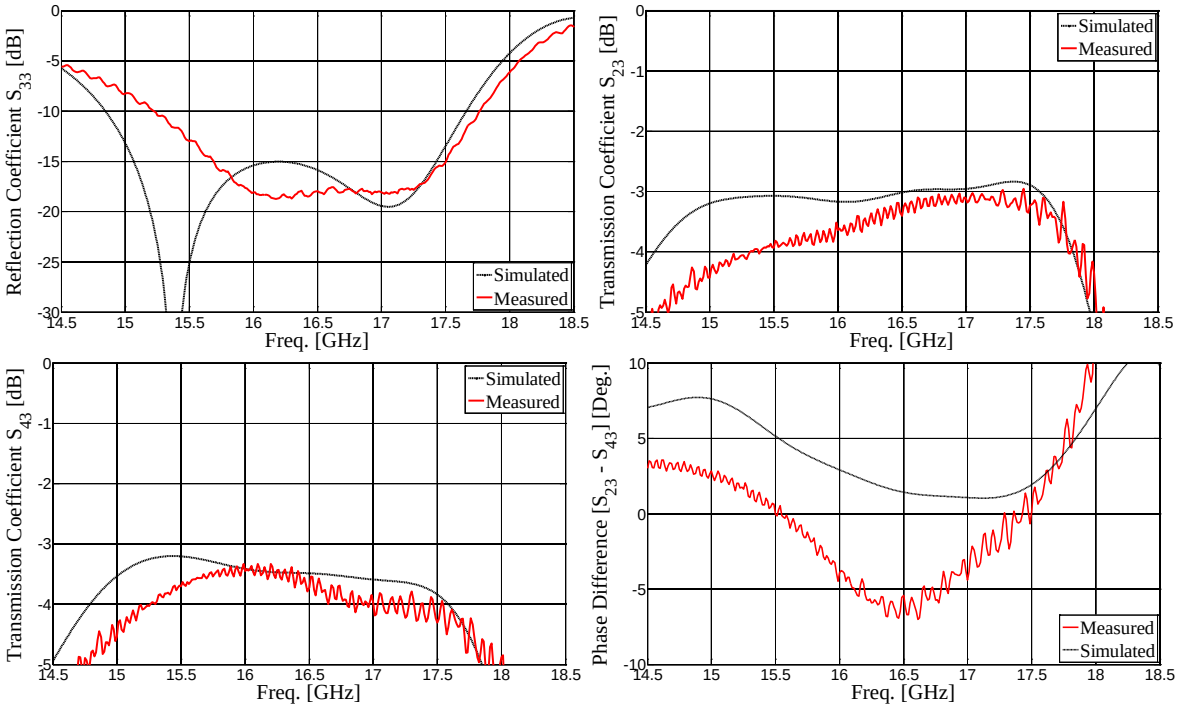

Figure 5. 13 Simulated & Measured S-parameters and phase difference of port 2 and port 4, when port 3 is input port.

Chapter 6

Microstrip-Ridge Gap Waveguide – study of losses, bends and transition to WR-15

In this chapter, we will show the design of microstrip-ridge gap waveguide, its wideband transition to WR-15 and in addition a theoretical and experimental study of the losses in the microstrip-ridge gap waveguide. The microstrip-ridge gap waveguide is designed by using a substrate with ground plane and shorting the inverted microstrip line periodically by via holes to the ground plane. The AMC layer is also created by a periodic pattern of via holes on the dielectric material used in [29]. The AMC-type via hole surface together with the upper metal surface produces a stopband for all parallel-plate modes, except for the quasi-TEM mode along the inverted microstrip line.

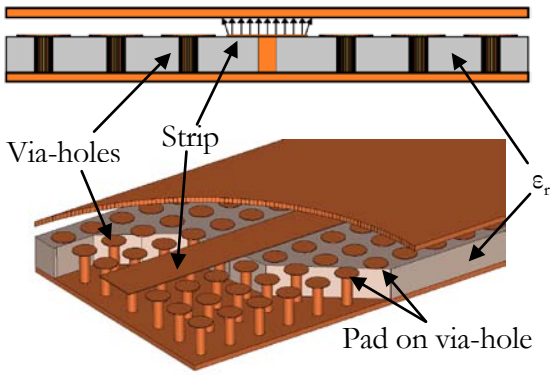

Figure 6. 1 Basic configuration of microstrip ridge gap waveguide.

6.1 Geometry and Modeling

The geometry of the microstrip-ridge gap waveguide with via holes is shown in Figure 6. 1. The strip at the surface of the substrate is connected to the ground plane through periodic via holes. The periodic pattern of via holes in the substrate on both sides of the microstrip creates a PMC layer that makes the waves propagating only in the narrow gap between the top metal plate and the microstrip, in the form of a quasi-TEM mode. The via holes work in a similar way to a pin surface, with pin height of 0.508 mm and diameter 0.25 mm. The diameter of the pad above the via hole is 0.7588 mm. The

distance between two vias is 1.0 mm. The substrate material is 0.508 mm thick Rogers RO3003 having ε_r equal to 3.0. The air gap is 0.25 mm. The dispersion diagram describes the major characteristics of the gap waveguide technology. By using the Eigen mode solver in CST microwave studio [56], the dispersion diagram is calculated as a function of frequency for the choice of dimensions of the gap waveguide, shown in Figure 6. 2a. We can see that the stopband of the parallel-plate modes for this specific case is between 45 and 72 GHz and within this band only a single mode is propagating.

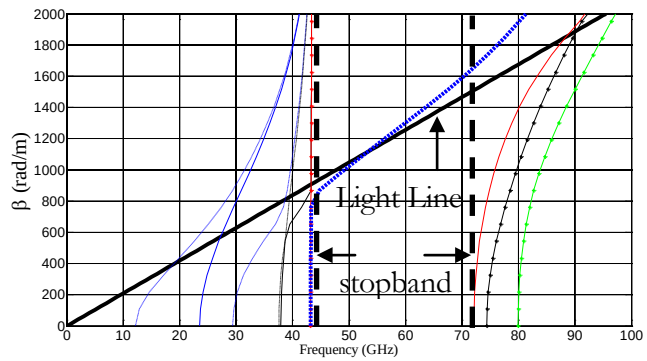

(a)

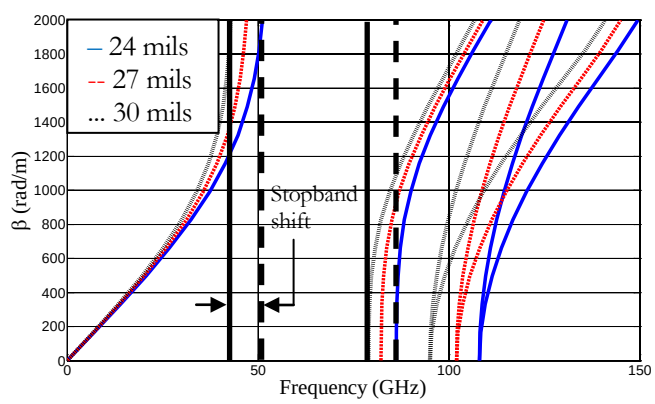

(b)

Figure 6. 2 a) Dispersion diagram of microstrip-ridge gap waveguide. b) Dispersion diagram of various pad diameters of single unit pin.

For the case of gap waveguide having metallic pins, the stopband is mainly controlled by the air gap, height, width and period of the pins [47]. In the present case the diameter of the pads on the top of the via hole pins, and the relative permittivity of the PCB, also affect the stopband. The pads appear due to the metallization process of the via-hole and this cannot be avoided. Figure 6. 2b shows a study

summarizing the effect of pad diameter. It can clearly be seen that, by keeping the period and via-hole diameter fixed, an increase in the pad diameter on the top of via-hole will shift the stopband toward the lower frequencies.

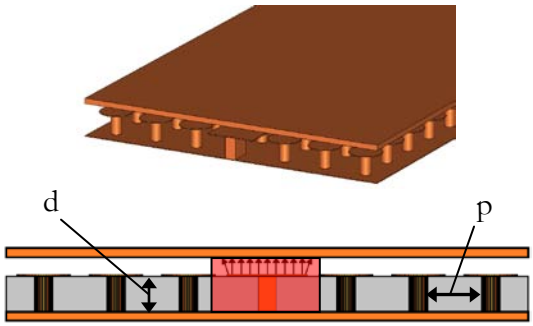

Figure 6. 3 Port definition for the microstrip ridge gap waveguide.

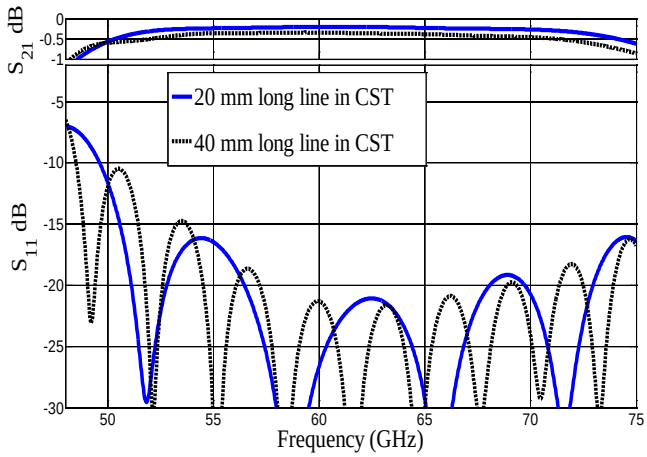

Figure 6. 4 Simulated S–parameters of the microstrip ridge waveguide.

6.2 Port definition and Simulated Results

The port definition for microstrip-ridge gap waveguide is not so easy in the sense that we need to modify the via-hole under the strip in front of the port. This modification has been done in order to match the port with the line and this is only for simulation purpose to excite the desired mode, as shown in Figure 6. 3. In Ansoft HFSS [66], the lumped port is found to be well matched with the line but the equivalent of this port in CST [56], is not so effective. So the procedure is that we define a small finite length rectangular block just in front of the port, started from the edge of the strip. The width of the rectangular block is supposed to be the same as that of the diameter of a via hole.

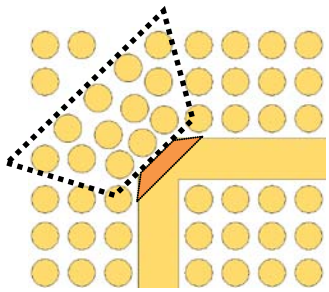

Figure 6. 5 Geometry of the 90° bend, with the area of tuned pins and portion of bend.

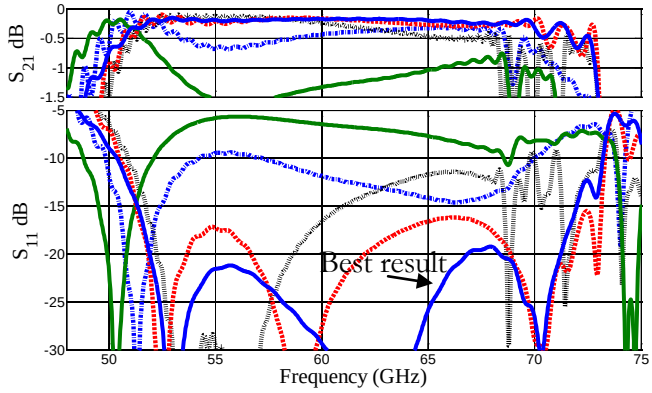

Figure 6. 6 Simulated S–parameters of the microstrip ridge waveguide 90° bend with tuning of pins location at the corner and mitered bend.

The simulated S-parameters are shown in Figure 6. 4. It can be seen that the reflection coefficient is below -20 dB over the desired bandwidth of 57-66 GHz and S_{21} is about -0.2 dB. This shows that the numerical ports are reasonably well matched with the line. The transmission coefficient become almost twice, if the length of the line is doubled, so there are noticeable ohmic losses in the line.

6.3 Design of 90° bend

Locations of via holes around 90° bend are very critical for making the bend work well. It is important to note that there is a minimum mechanical spacing which is allowed between the via-holes determined by the manufacturing process. At the same time the via-holes at the corner of the bend must be close enough to each other to avoid any resonant cavities, which we know from the Eigen mode unit cell simulations. Inside the highlighted area in Figure 6. 5, the locations of the via-holes are tuned to attain the lowest S_{11} and highest S_{21} over the whole bandwidth. Similarly, the discontinuity created by the bend also needs to be adjusted by the mitering in order to minimize its effect. Simulated S-parameters are shown in Figure 6. 6, for this particular bend. Again, the simulated S_{11} is below -20 dB over 57-66 GHz and S_{21} is about -0.2 dB.

6.4 Comparison between Microstrip-ridge gap line, Normal Microstrip Line and Inverted Microstrip Line

Microstrip lines are most commonly used in microwave integrated circuits [67]. Microstrip line losses have usually been treated as conductor and dielectric losses. In addition, there are also radiation losses due to discontinuities (such as open circuits, short circuits and bends) and losses due to surface waves [67]. The latter is in particular large for large substrate thicknesses. Dielectric losses do not depend on the thickness of the substrate and its dimensions, whereas the conductor losses reduce inversely proportional to the line width (for constant line impedance). The conductor losses include the actual conductance of the material, frequency dependent skin effect losses (if the conducting strips consists of layers of material of different conductivity like surface treatment of Copper), and losses due to the roughness of the surface (random scratches and bumps) [68].

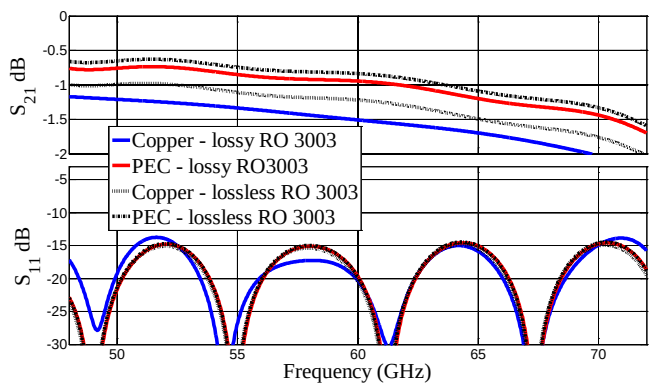

Figure 6. 7 S-parameters of microstrip line, with lossy/lossless conductor and lossy/lossless dielectric.

Figure 6. 7 shows an example of the losses suffered by a 3 cm long microstrip line with two 90° bends when realized with different combinations of materials. Obviously, the best is the case when the conductor is PEC and the dielectric material is lossless. The "lossless" substrate cases in this and later graphs are simply modeled by setting the loss tangent of the material to zero. The transmission coefficient for this case is about -0.75 dB at 60 GHz. Since the material is lossless, the main contributors to the losses are surface wave and radiation losses at the bends. The loss increases by 0.5 dB, if we use copper instead of PEC. This is much higher than the case when the dielectric becomes lossy and the conductor remains PEC. Together with lossy dielectric and copper, the losses increased by nearly 0.75 dB everywhere within the bandwidth. This example clearly shows that the combined

losses due to the conductor and the surface waves and radiation are larger than the losses due to the dielectric at high frequencies.

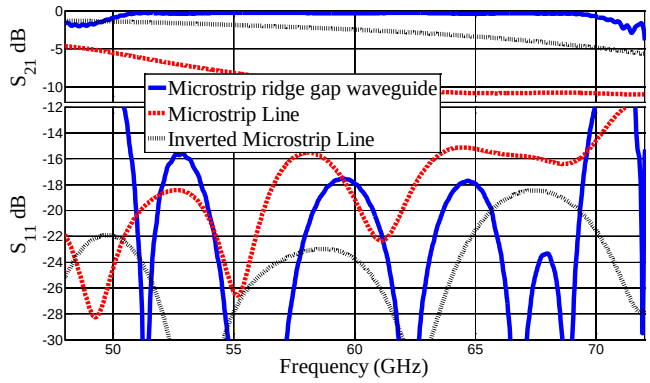

Figure 6. 8 Simulated S_{11} and S_{21} of two 90° bend of microstrip ridge gap waveguide, microstrip line and inverted microstrip line of similar width

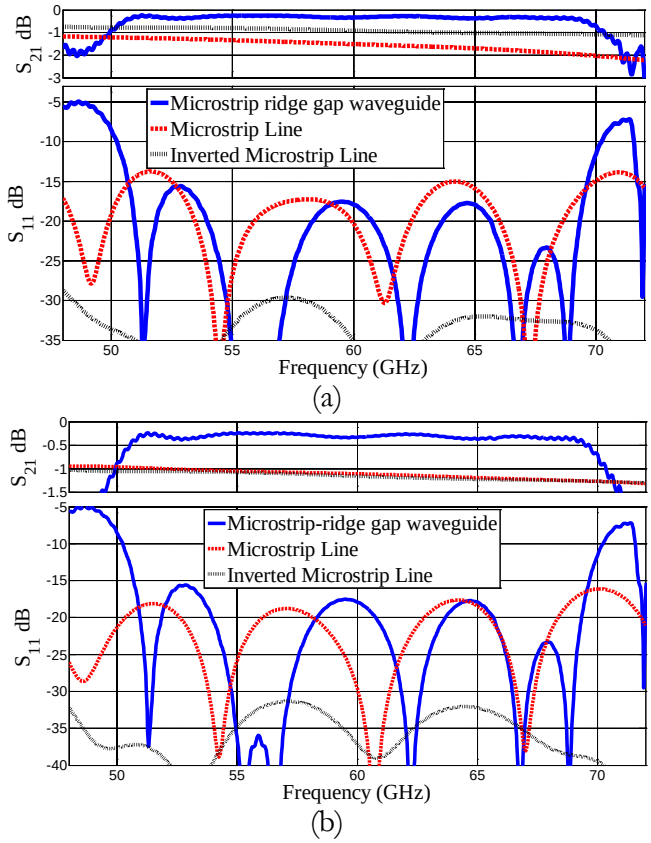

Figure 6. 9 Simulated S_{11} and S_{21} of two 90° bend of microstrip ridge gap waveguide, microstrip line and inverted microstrip line. (a) Width of microstrip line and inverted microstrip line is half as before. (b) Width of microstrip line and inverted microstrip line is quarter as before.

Similarly, the inverted microstrip line can be used as a low loss line [69]. Figure 6. 8 shows also the simulated S_{11} and S_{21} of microstrip line and inverted microstrip line of similar strip width as well as air

gap / length as the microstrip-ridge gap waveguide. The width of the strip and air gap is 1.1176 mm and 0.25 mm, respectively. It can clearly be seen that, with the same widths, microstrip-ridge gap waveguide has much lower transmission losses. The losses can be reduced in microstrip line and inverted microstrip line, if decrease the width of the line by half and quarter as that microstrip-ridge gap waveguide, but the microstrip-ridge gap waveguide is still much better. The results are shown in Figure 6. 9.

6.6 Dielectric losses in Microstrip-ridge gap waveguide

In this section we will study the effect of dielectric with higher ε_r on the transmission losses of microstrip ridge gap waveguide. For this purpose we have chosen three dielectric materials, i.e. RO3003, RT/duroid 5880 and FR4. The permittivity and the loss tangent of each material are summarized in Table 6. 1.

Material	Relative Permittivity	Loss Tangent	Standard thickness used
RT 5880	2.2	0.0009	0.787 mm
RO 3003	3.0	0.0013	0.508 mm
FR4	4.7	0.018	0.508 mm

Table 6. 1 Material used for loss comparison.

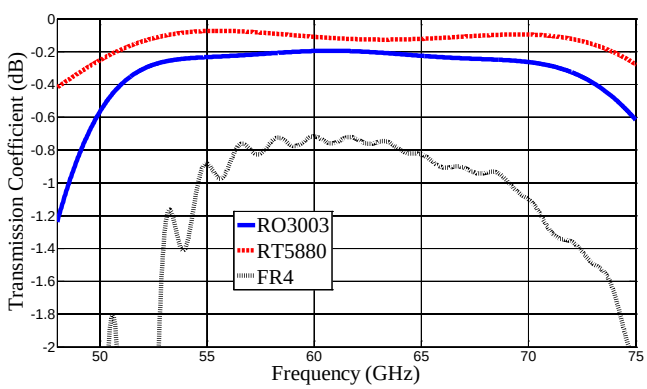

Figure 6. 10 Transmission coefficient of microstrip ridge gap waveguide with different dielectric material.

The transmission coefficients, shown in Figure 6. 10, clearly indicate that with higher dielectric value and loss tangent, the losses are larger. Figure 6. 11 shows an example of transmission coefficient of microstrip-ridge gap waveguide, using FR4 as dielectric material. The length of the line is very small, i.e. 1.5 cm, and the width of the line is 1.3 mm. S_{21} for the lossless material is about -0.2 dB. Unlike with example shown in Figure 6. 7, in microstrip-ridge gap waveguide, the main contributor of the

losses in the line is the dielectric material if this is chosen as FR4 which is a low cost material, even with the wider strips. This proves one of the main advantages of using microstrip-ridge gap waveguide: at 60 GHz and above it is possible to make circuits with wider width of the strip line than for microstrip line and inverted microstrip line.

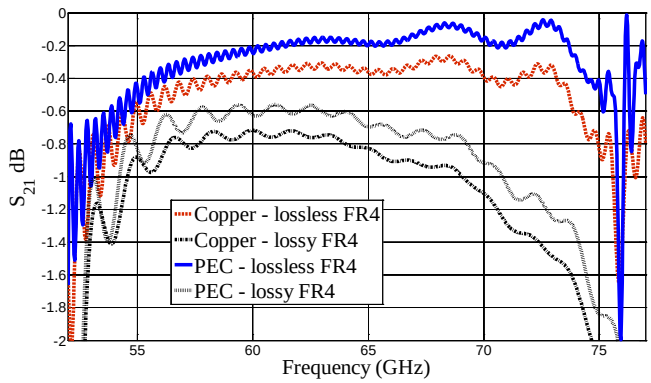

Figure 6. 11 Transmission coefficients of microstrip-ridge gap waveguide simulated on FR4 dielectric.

6.7 Transition with WR-15

Figure 6. 12 shows the basic drawing of the chosen vertical microstrip-ridge gap waveguide to WR-15 transition. The rectangular waveguide is connected from the bottom of the microstrip-ridge gap waveguide. This configuration will enable us to establish a feeding network of an antenna excited via coupling slots in the upper smooth plate. However, the design of it is not straight-forward because we have the planar limitations of the PCB geometry.

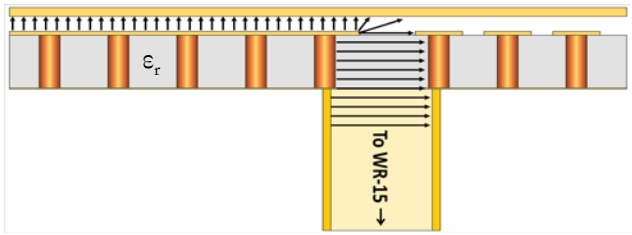

Figure 6. 12 Side view of basic configuration of microstrip ridge gap waveguide to WR-15 transition.

For this purpose, we make a matching stub at the end of the microstrip-ridge line. This stub is also connected to the ground plane through a via-hole as shown in Figure 6. 13a. With fine tuning of the location of via-holes around WR-15 and the width / length of the stub, shown in Figure 6. 13b, we were able to match the microstrip-ridge gap waveguide with WR-15 over the desire bandwidth of 57-66 GHz.

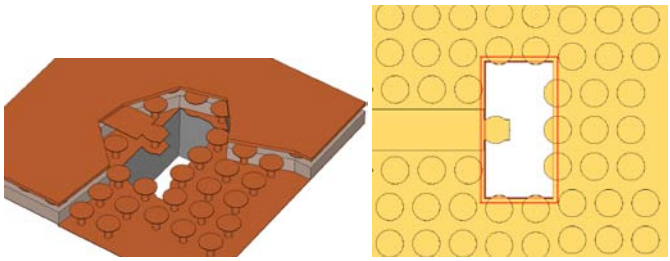

(a) (b)

Figure 6. 13 Transition design, a) Side view, b) Top view.

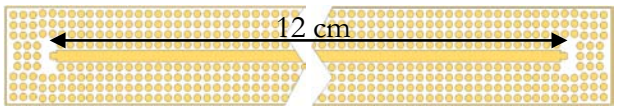

(a)

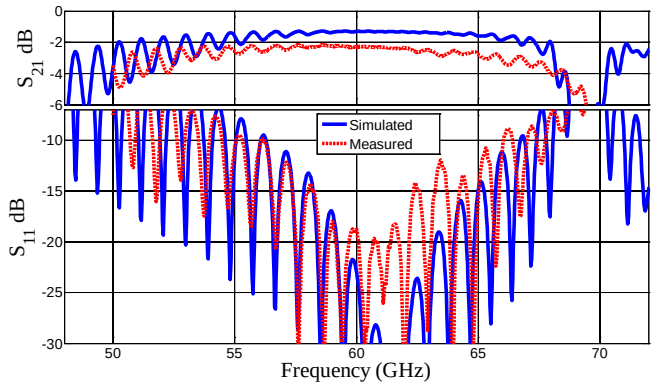

(b)

Figure 6. 14 Microstrip ridge gap waveguide to WR-15 transition. a) 12 cm back-to-back configuration. b) S-parameters of the structure.

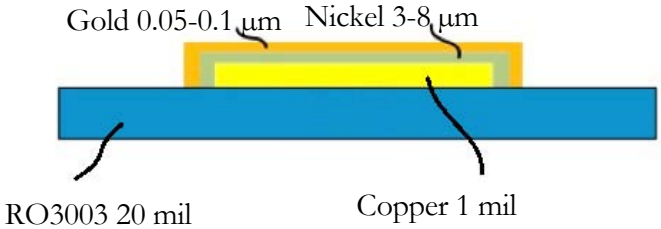

Figure 6. 15 Cross section view of the Microstrip-ridge line, with nickel and gold.

Figure 6. 14a shows a 12 cm long back-to-back microstrip-ridge gap waveguide to WR-15 transition. The simulated and measured S-parameters (Figure 6. 14b) show that the reflection coefficient is below -10 dB between 56 – 67 GHz. This means that the single transition will be better than -15 dB over this band. Similarly the simulated S_{21} is about -1.5 dB over the desired bandwidth, whereas this loss is about

0.7 dB higher in the measurements. We believe that this difference in transmission coefficient is due to misalignment and tolerances in the mechanical structure. During simulation we made microstrip-ridge with only pure lossy copper, but the manufactured one includes silver plating. We have also made one prototype having 3-8 μm nickel and then 0.05-0.1 μm gold layer, i.e. ENIG plating as shown in Figure 6. 15. But the transmission coefficient is below -4.2 dB in that case, which is very low in comparison to the simulated results. Similarly, we also make a two 90° bend of the microstrip ridge gap waveguide with transition and is shown in Figure 6. 16a. The size of two 90° bend is 8.3 cm x 4.3 cm, so the path for wave propagation is almost 12 cm long similar to that we have made for straight line. The simulated and measured S_{11} is below -10 dB between 56 – 67 GHz and the simulated S_{21} is around -1.5 dB, whereas the measured transmission coefficient is about -2.5 dB, which also include losses due to two 90° bends.

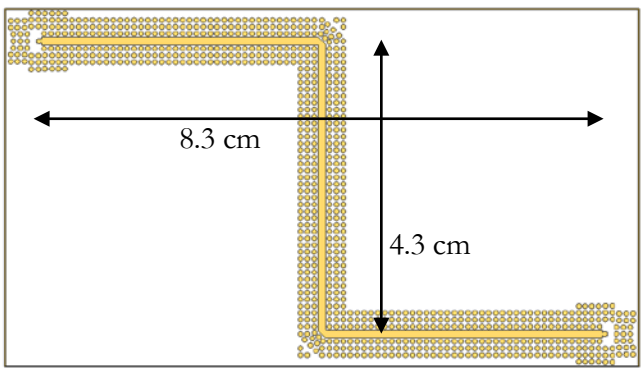

(a)

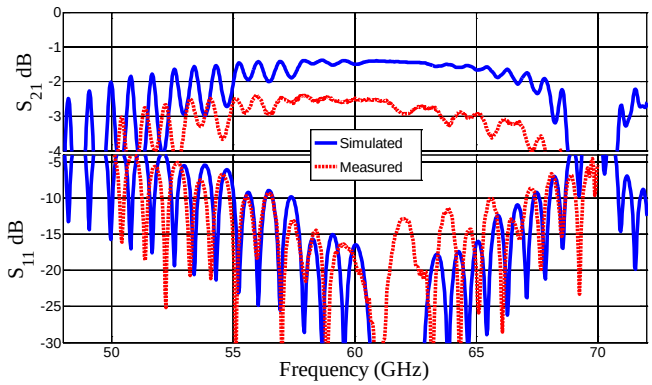

(b)

Figure 6. 16 Two 90° bends of microstrip ridge gap waveguide to WR-15 transition. a) 8.3 cm x 4.3 cm back-to-back configuration. b) S-parameters of the structure.

Chapter 7

UWB Power Divider, packaged with Gap Waveguide Technology

The feeding network is always a critical part in the design of the Eleven antenna. Good UWB performance of a low reflection coefficient and low ohmic loss, a compact simple geometry and low cost make the design a real challenge. One alternative of feeding networks for the Eleven antenna is to employ the UWB passive baluns [70], plus two UWB 3-dB power divider, shown in Figure 7. 1. By this feeding network, the 4 differential ports of the Eleven feed are transformed to 2 single ended ports, one for each polarization.

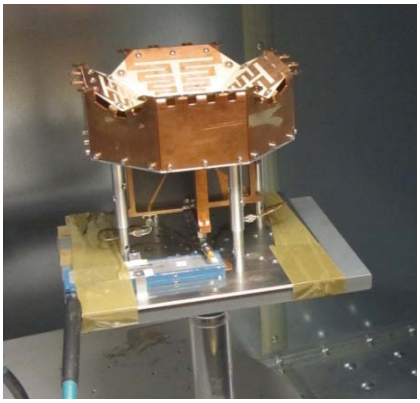

Figure 7. 1 Eleven Antenna with passive balun solution and power combiner

In addition to the high loss, the conventional packaging for UWB power dividers, simply enclosing the device in a metallic box, may also cause resonances. This will eventually degrade the performance of the whole system. The purpose is to develop a small and low loss power divider with a bandwidth in the order of 10:1. By reducing the size, when it is enclosed in a metal box, the power divider may have resonances only at higher frequencies of the bandwidth. These resonances can then be suppressed by using the gap waveguide technology, made by bed of nails [45], see Figure 7. 2. Both simulated and measured reflection and transmission coefficients are in good agreement between 1–12 GHz, see

Figure 7. 3-Figure 7. 5. Although simulated results extend the behavior up to 13.5 GHz. This may be because of the mechanical inaccuracy in the milling process for the manufactured one.

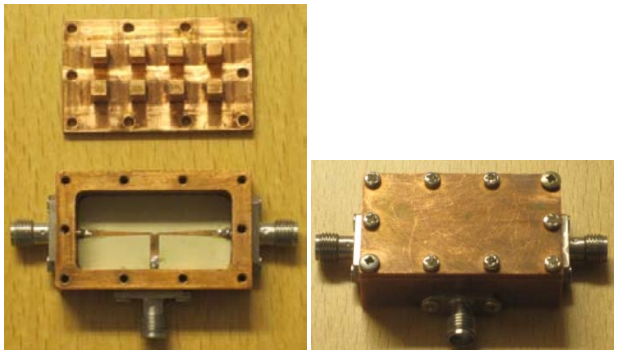

Figure 7. 2 Photo of the 1–13.5 GHz power divider with bed-of-nails.

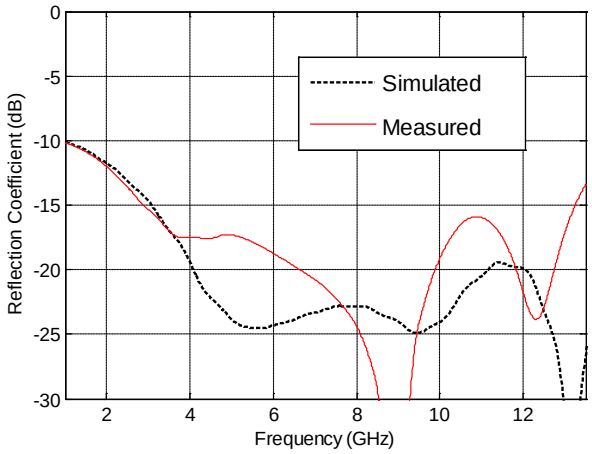

Figure 7. 3 Simulated and measured reflection coefficient of the power divider package with bed-of-nails.

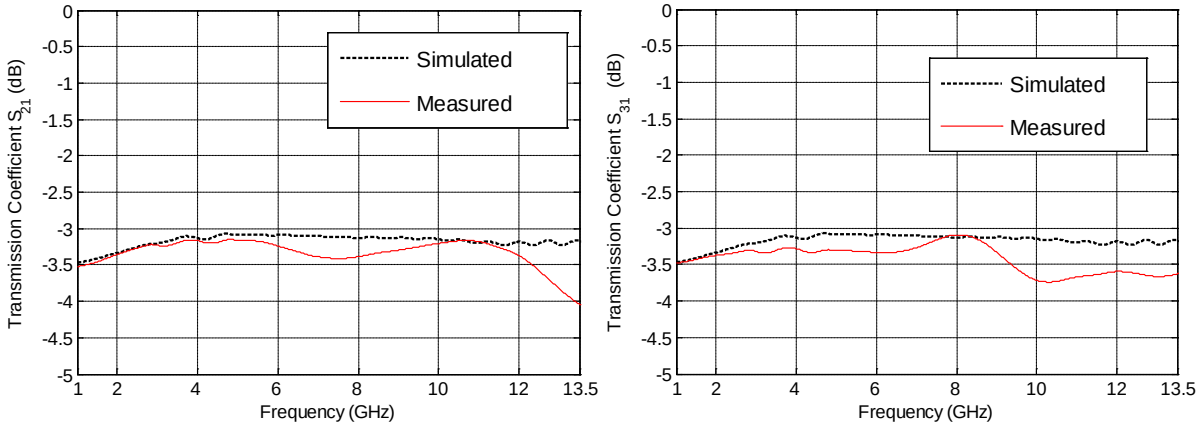

Figure 7. 4 Simulated and measured transmission coefficient of the power divider package with the bed-of-nails

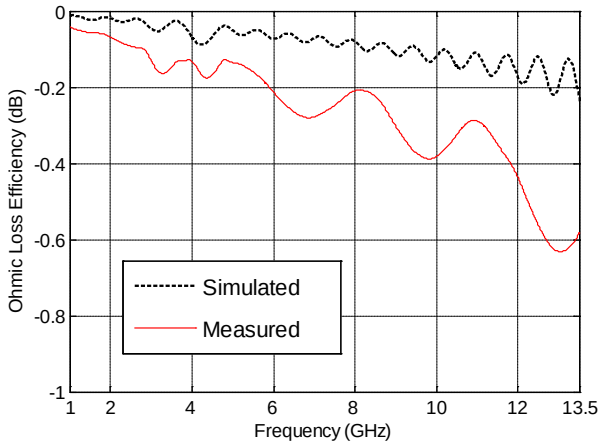

Figure 7. 5 Simulated and measured ohmic losses of the power divider.

Chapter 8

Conclusion

In the first topic of this thesis, a new compact UWB passive balun solution for the decade bandwidth Eleven antenna has been presented, based on using four printed circuit boards located vertically to the ground plane on the back side of it. The solution seems feasible for the requirements of the Eleven feed. The lower frequency of the operation is limited by the length of balun. There were two versions of the feeds that have been developed. The first version, linear tapering, has aperture efficiencies better than -2.5 dB between 2 – 12 GHz and around -3 dB between 12 – 14 GHz. Although the second version, K-tapering, has lower efficiency at few frequency points between 8–9 GHz, but it has better reflection coefficient than the linear tapering balun, i.e. less than -10 dB. This formation of balun will transform four differential ports to four single ended 50 ohm ports. It is also then possible to reduce these numbers of ports to two single ended ports, one for each polarization. A UWB power combiner is also presented to fulfill this requirement. This power combiner is based on simple T-junction packaged by using gap waveguide technology. A rigorous feeding network correction method for determining the radiation efficiency of a multiport antenna based on measurements has also been presented. This method removes the losses in the multiport feeding network from the total radiation efficiency, when there are multiple reflections between the antenna and the feeding network due to the mismatch between them. The measured radiation efficiency is about -0.5 dB.

In the second topic, we have presented a 4-port self-grounded bowtie antenna. The antenna is very simple and can be used for both MIMO application and LOS antenna systems. The reflection coefficient is below -10 dB between 1.5 and 3.0 GHz. The total radiation efficiency is high when the antenna is differentially excited, and it is mainly due to the mismatch factor. The radiation pattern is stable and the maximum beam direction is in the normal to the ground plane so it can be used to feed a reflector as well.

In the third topic of this thesis, numerical studies have been done to determine the characteristic impedance and wave impedance of ridge gap waveguide and groove gap waveguide, respectively. This analysis is based on the port impedance and reflection coefficient provided by the commercial code for

waveguide ports. The results show that within most of the stopband of the parallel-plate modes, both gap waveguides and their equivalent hollow waveguides are performing relatively close to each other. The air gap between the top metal and the ridge is the key parameter and should be made as smaller as possible for the mode to propagate as more closely to that of light line.

We have also done numerical studies of the microstrip-ridge gap waveguide realized in a PCB. The ridge is realized by a metal strip with metalized via-holes, and the AMC pin surface is realized by metallized via-holes with a pad at the top. The results have been compared with the conventional microstrip line and the inverted microstrip line, and we found that the microstrip-ridge gap waveguide has much lower losses. The reasons are that there is no substrate in the air gap region where the waves propagate, and that we can use much wider metal strip without having problems with radiation and surface waves. We have also presented a transition from microstrip-ridge gap waveguide to WR-15. The performances were verified in a back-to-back configuration with both a straight microstrip-ridge gap waveguide line as well as one with two 90° bends. The verification showed that the measured losses are about 50% larger than the simulated results, and that the two 90° bends cause a doubling of the losses. Except for the higher losses, the performance looks as expected.

Bibliography

[1] B. A. Kramer, C.-C. Chen, M. Lee, and J. L. Volakis, "Fundamental Limits and Design Guidelines for Miniaturizing Ultra-Wideband Antennas", IEEE Antennas and Propagation Magazine, Vol. 51, No.4, August 2009.

[2] C. C. Chen, "Ultrawide Bandwidth Antenna Design", in J. L. Volakis (ed.), Antenna Engineering Handbook, Fourth Edition, McGraw-Hill, Inc., 2007, Chapter 19, pp. 19-2.

[3] D. Nyberg, P.-S. Kildal, J. Carlsson, "Effects of intrinsic radiation Q on mismatch factor of three types of small antennas: single-resonance, gradual-transition and cascaded-resonance types", IET Microwaves, Antennas & Propagation, vol. 4, No. 1, pp. 83-90, January 2010.

[4] J. Yang and A. Kishk, "A novel low-profile compact directional ultra-wideband antenna: The self-grounded Bow-Tie antenna", IEEE Trans Antennas Propag. vol.60, pp. 1214–1220.

[5] W. Wiesbeck, G. Adamiuk, C. Sturm, "Basic Properties and Design Principles of UWB Antennas", Proceedings of the IEEE, vol. 97, No. 2, pp. 372-385, February 2009.

[6] A. Zamanifekri and J. Yang, "Two octaves bandwidth passive balun for the Eleven feed for reflector antennas", 2010 IEEE international Symp. on Antennas Propag., Toronto, Ontario, Canada, July 11-17, 2010.

[7] R. Olsson, P.-S. Kildal, S. Weinreb, "The Eleven antenna: a compact low-profile decade bandwidth dual polarized feed for reflector antennas", IEEE Transactions on Antennas and Propagation, vol. 54, no. 2, pt. 1, pp. 368-375, Feb. 2006.

[8] R. Olsson, P.-S. Kildal, and M. Shields, "Measurements of a 150 to 1700 MHz low loss Eleven feed for the 42 m radio telescope at Green Bank", IEEE AP-S International Symposium, Albuquerque, N.M., July 2006.

[9] P.-S. Kildal, R. Olsson and J. Yang, "Development of three models of the Eleven antenna: a new decade bandwidth high performance feed for reflectors"", In 1st Eur. Conf. on Antennas Propagat. (EuCAP2006), Nice, France, 6-10 November 2006.

[10] Y. B. Karandikar and P.-S. Kildal, "Optimization of 200-800 MHz Eleven feed for use in reflector antennas of GMRT", The Second European Conference on Antennas and Propagation (EuCAP 2007), Edinburgh, 11 - 16 November 2007.

[11] J. Yang, X. Chen, N. Wadefalk, P.-S. Kildal, "Design and realization of a linearly polarized Eleven feed for 1-10 GHz", IEEE Antennas and Wireless Propagation letters (AWPL), Vol. 8, pp. 64-68, 2009.

[12] J. Yang, P.-S. Kildal, "Optimization of Reflection Coefficient of Large Log-Periodic Array by Computing Only a Small Part of It", IEEE Trans. on Antennas Propag., vol. 59, no. 6, pp.1790-1797, June 2011.

[13] Jian Yang, Miroslav Pantaleev, Per-Simon Kildal and Leif Helldner, "Design of compact dual-polarized 1.2-10 GHz Eleven feed for decade bandwidth radio telescopes", IEEE Trans. on Antennas Propagat., vol. 60, no. 5, pp. 2210–2218, May 2012.

[14] J. Yin, J. Yang, M. Pantaleev, and L. Helldner, "The circular Eleven antenna: a new decade-bandwidth feed for reflector antennas with high aperture efficiency", to appear in IEEE Trans. Antennas Propagat., vol. 61, 2013.

[15] V. Rodriguez, "An open-boundary quad-ridged guide horn antenna for use as a source in antenna pattern measurement anechoic chambers," IEEE Antennas and Propagation Magazine, Vol. 48, No. 2, pp. 157-160, Apr. 2006.

[16] G. Cortes-Medellin, "Novel non planar ultra wide band quasi self complementary antenna", Proc. of IEEE AP-S Symposium, Honolulu, Hawaii, 9-15 June 2007, pp. 5733 – 5736.

[17] S. Bruni, A. Neto and F. Marliani, " The Ultrawideband leaky lens antenna," IEEE Trans. Antennas Propogat., vol. 55, no.10, pp. 2642-2653, Oct. 2007.

[18] J. Yin, J. A. Aas, J. Yang, and P.-S. Kildal, "Monopulse tracking performance of multi-port Eleven antenna for use in terminals for satellite communications." The 2nd Eur. Conference on Antennas and Propagation (EuCAP 2007), Edinburgh, 11 - 16 November 2007.

[19] X. Chen, P.-S. Kildal, J. Carlsson, and J. Yang, "Comparison of ergodic capacities from wideband MIMO antenna measurements in reverberation chamber and anechoic chamber," IEEE Antennas Wireless Propag. Lett., vol. 10, pp. 446–449, 2011.

[20] J. Yang, S. Pivnenko, T. Laitinen, N. Jamaly, and J. Carlsson, "Measurements of diversity gain and radiation efficiency of the Eleven antenna by using different measurement techniques." Barcelona: 4th European Conference on Antennas and Propagation, (EuCAP 2010), April 2010.

[21] Y. B. Karandikar, P. -S. Kildal, " Comparisons of different descrambler/power combining boards layout for multi-port, decade bandwidth Eleven feed ", The Fourth European Conference on Antennas and Propagation (EuCAP 2010), Barcelona, 12-16 April 2010.

[22] J. Yang, M. Pantaleev, P.-S. Kildal, B. Klein, Y. Karandikar, L. Helldner, N. Wadefalk, and C. Beaudoin, "Cryogenic 2–13 GHz Eleven Feed for Reflector Antennas in Future Wideband Radio Telescopes", IEEE Transactions on Antennas and Propagation, Vol. 59, No. 6, June 2011, pp. 1918-1934.

[23] C. A. Balanis, Antenna Theory Analysis and Design, 3rd Edition, p. 538, John Wiley & Sons, Inc., 2005.

[24] Y.Ding, Z. W. Du, K. Gong,and Z. H. Feng,"A novel dual-band printed diversity antenna for mobile terminals," IEEE Trans. Ant. Propag., vol. 55, no. 7, pp. 2088–2096, Jul. 2007.

[25] J.-F. Li, Q.-X. Chu, and T.-G. Huang, "A Compact Wideband MIMO Antenna With Two Novel Bent Slits", IEEE Trans. on Antennas and Propagation, Vol. 60, No. 2, February 2012.

[26] P.-S. Kildal and K. Rosengran, "Correlation and capacity of MIMO systems and mutual coupling, radiation efficiency, and diversity gain of their antennas: Simulations and measurements in a reverberation chamber," IEEE Commun. Mag., vol. 42, no. 12, pp. 102–112, Dec. 2004.

[27] K. Rosengran and P.-S. Kildal, "Radiation efficiency, correlation, diversity gain and capacity of a six-monopole antenna array for a MIMO system: Theory, simulation and measurement in reverberation chamber," IEE Proc. Microw. Ant. Propag. , vol. 152, no. 1, pp. 7–16, 2005.

[28] P.-S. Kildal, E. Alfonso, A. Valero-Nogueira, E. Rajo-Iglesias, "Local metamaterial-based waveguides in gaps between parallel metal plates", IEEE Antennas and Wireless Propagation letters (AWPL), Volume 8, pp. 84-87, 2009.

[29] E. Pucci, E. Rajo-Iglesias, P.-S. Kildal, "New Microstrip Gap Waveguide on Mushroom-Type EBG for Packaging of Microwave Components", IEEE Microwave and Wireless Components Letters, Vol. 22, No. 3, pp. 129-131, March 2012.

[30] P.-S. Kildal, A. U. Zaman, E. Rajo-Iglesias, E. Alfonso, A. Valero-Nogueira, "Design and experimental verification of ridge gap waveguide in bed of nails for parallel-plate mode suppression", IET Microwave, Antennas & Propagation, Volume 5, Issue 3, pp. 262-270, 2011.

[31] M. Basraoui and Prasad N. Shastry, "Wideband, Planar, Log-Periodic Balun", IEEE MTT-S International Microwave Symposium Digest, Baltimore, June 1998, pp. 785-788.

[32] Z-Yu Zhang, Y-Xin Guo, L. C. Ong, and M. Y. W. Chia, "A New Wide-band Planar Balun on a Single-Layer PCB", IEEE Microwave & Wireless Components Letters, Vol. 15, No. 6, pp. 416-418 , June 2005.

[33] R. Jacques, D. Meignant, "Novel Wide Band Microstrip Balun ", Proc. of 11th European Microwave Conference, 7-11 September 1981, pp. 839-843.

[34] X. Lan, F. Fong, M. Kintis, K. Kono, D. Yamauchi, W.-B. Luo, and D. Farkas, "An Ultra-Wideband Balun Using Multi-Metal GaAs MMIC Technology", IEEE Microwave and Wireless Components Letters, Vol. 20, No. 8, pp. 474-476, August 2010.

[35] M. E. Bialkowski and A. M. Abbosh, "Design of a Compact UWB Out-of-Phase Power Divider", IEEE Microwave and Wireless Components Letters, Vol. 17, No. 4, April 2007, pp. 289-291.

[36] A. M. Abbosh and M.E. Bialkowski, "An UWB Planar Out-of-Phase Power Divider Employing Microstrip-Slot and Parallel Stripline-Microstrip Transitions", IJMOT International Journal of Microwave and Optical Technology, Vol. 2, No. 2, April 2007, pp. 87-90.

[37] Y.-G. Kim, D.-S. Woo, K. W. Kim, Y.-K. Cho, "A New Ultra-wideband Microstrip-to-CPS Transition", IEEE/MTT-S International Microwave Symposium, 3-8 June 2007, pp. 1563-1566.

[38] J. Chramiec and B. J. Janiczak, "Design of impedance-transforming microstrip-balanced stripline tapered transitions", Electronics Letters 7th January 1993 Vol. 29 No. 1, pp. 3-4.

[39] J. Yang and A. Kishk, "The Self-Grounded Bow-Tie Antenna", 2011 IEEE International Symposium on Antennas and Propagation, Spokane, USA, 3-8 July, 2011, pp. 1452-1455.

[40] J. Yang and A. Kishk, "A Novel Low-Profile Compact Directional Ultra-Wideband Antenna: the Self-Grounded Bow-Tie Antenna", IEEE Transactions on Antennas and Propagation, vol. 60, issue 3, March 2012, pp. 1214-1220.

[41] G. H. Brown and O. M. Woodward, "Experimentally determined radiation characteristics of conical and triangular antennas," RCA Rev., pp. 425-452, Dec. 1952.

[42] P. J. Gibson, "The Vivaldi aerial," Proc. 9th European. Microwave Conference, pp. 101-105, 1979.

[43] ETS-Lindgren horn; http://www.ets-lindgren.com/pdf/3164-05.pdf

[44] E. Rajo-Iglesias, A. U. Zaman, P.-S. Kildal, "Parallel plate cavity mode suppression in microstrip circuit packages using a lid of nails", IEEE Microwave and Wireless Components Letters, Vol. 20, No. 1, pp. 31-33, Dec. 2009.

[45] A. U. Zaman, J. Yang, and P.-S. Kildal, "Using Lid of Pins for Packaging of Microstrip Board for Descrambling the Ports of Eleven Antenna for Radio Telescope Applications", 2010 IEEE international Symp. on Antennas Propag., Toronto, Ontario, Canada, July 11-17, 2010.

[46] P.-S. Kildal, "Three metamaterial-based gap waveguides between parallel metal plates for mm/submm waves", 3rd European Conference on Antennas and Propagation, 2009. EuCAP 2009. Berlin, Germany, 23-27 March 2009.

[47] E. Rajo-Iglesias, P.-S. Kildal, "Numerical studies of bandwidth of parallel plate cut-off realized by bed of nails, corrugations and mushroom-type EBG for use in gap waveguides", IET Microwaves, Antennas & Propagation, Vol. 5, No 3, pp. 282-289, March 2011.

[48] O. M. Woodward, S. M. Perlow, "Balance Quality Measurements on Baluns", IEEE Transactions on Microwave Theory and Techniques, Vol. 31, No. 10, October 1983, pp. 821-824.

[49] Bluetest Reverberation Test System, http://www.bluetest.se.

[50] H. Raza, J. Yang: 'Compact UWB Power Divider Packaged by Using Gap-Waveguide Technology', 6th Eur. Conf. On Antennas and Propagation (EuCAP 2012), Prague, Czech Republic, 26 – 30 March 2012.

[51] P.-S. Kildal, "Factorization of the feed efficiency of paraboloids and Cassegrain antennas," IEEE Transactions on Antennas and Propagations, vol. 33, No. 8, pp. 903-908, August 1985.

[52] P.-S. Kildal, Z. Sipus, "Classification of Rotationally Symmetric Antennas as Types BOR0 and BOR1", IEEE Antennas and Propagation Magazine, vol. 37, No 6, pp. 114, December 1995.

[53] J. Yang, "On Conditions for Constant Radiation Characteristics for Log-Periodic Array Antennas," IEEE Transactions on Antennas and Propagation, vol. 58, No. 5, May 2010, pp. 1521-1526.

[54] J. Yang, S. Pivnenkoy and P.-Simon Kildal, "Comparison of two decade-bandwidth feeds for reflector antennas: the Eleven antenna and quadridge horn", In 4th Eur. Conf. on Antennas Propagat. (EuCAP2010), Barcelona, Spain, 12 - 16 April 2010.

[55] M. V. Ivashina, M. Ng Mou Kehn, P.-S. Kildal and R. Maaskant, "Decoupling efficiency of a wideband Vivaldi focal plane array feeding a reflector antenna", IEEE Transactions on Antennas and Propagation, Vol. 57, No. 2, pp 373-382, February. 2009.

[56] CST Microwave Studio, 3D EM Simulation Software. Computer Simulation Technology, Framingham, MA, 2012 [Online]. Available: http://www.cst.com.

[57] P.-S. Kildal, Foundations of Antennas – A Unified Approach, 2nd Edition, p. 70, Studentlitteratur, 2000.

[58] A. Polemi, S. Maci, "Closed form expressions for the modal dispersion equations and for the characteristic impedance of a metamaterial-based gap waveguide", IET Microw. Antennas Propag., 2010, Vol. 4, Iss. 8, pp. 1073–1080.

[59] E. Alfonso, P.-S. Kildal, A. Valero-Nogueira, M. Baquero, "Study of the characteristic impedance of a ridge gap waveguide", IEEE Antennas and Propagation Society International Symposium APSURSI'09, pp. 1-4, June 2009.

[60] E. Alfonso, M. Baquero, A. Valero-Nogueira, J.I. Herranz, P.-S. Kildal, "Power divider in ridge gap waveguide technology", 4th European Conference on Antennas and Propagation (EuCAP 2010), Barcelona, Spain, 12-16 April 2010.

[61] C. Volmer, M. Şengul, J. Webew, R. Stephan, M. A. Hein, "Broadband Decoupling and Matching of a Super directive Two-Port Antenna Array", IEEE Antennas and Wireless Propagation Letters, Vol. 7, 2008.

[62] J. Yang, and H. Raza, "Empirical Formulas For Designing Gap-Waveguide Hybrid Ring Coupler", Microwave and Optical Technology Letters, Vol. 55, Issue 8, pp. 1917–1920, August 2013.

[63] A. Algaba Brazález, A. Uz Zaman, P.-S. Kildal, "Improved Microstrip Filters Using PMC Packaging by Lid of Nails", IEEE Transactions on Components, Packaging and Manufacturing Technology, Vol. 2, No. 7, July 2012.

[64] S. A. Razavi, P.-S. Kildal, L. Xiang and E. Alfonso, "2×2-slot Element for 60GHz Planar Array Antenna Realized on Two Doubled-sided PCBs Using SIW Cavity and EBG-type Soft Surface fed by Microstrip-Ridge Gap Waveguide", submitted to IEEE Transactions on Antennas and Propagation, November 2013.

[65] E. Pucci, E. Rajo-Iglesias, J.-L. Vazquez-Roy and P.-S. Kildal, "Planar Dual-Mode Horn Array with Corporate-Feed Network in Inverted Microstrip Gap Waveguide", submitted to IEEE Transactions on Antennas and Propagation, Aug. 2013.

[66] Ansoft HFSS, 2009 [Online], version 12. Available: http://www.ansoft.com/.

[67] E. J. Denlinger, "Losses of Microstrip Lines", IEEE Trans. on Microwave Theory Techniques, VOL. MTT-28, NO. 6, 1980.

[68] R. A. Pucel, D. J. Masse and C. P. Hartwig, "Losses of Microstrips", IEEE Trans. on Microwave Theory Techniques, VOL. MTT-16, NO. 6, 1968.

[69] R. S. Tomar and P. Bhartia, "Suspended and Inverted Microstrip Design", Microwave Journal, March 1986, pp. 173-177.

[70] H. Raza, J. Yang and M. Pantaleev, "A compact UWB passive balun solution for cryogenic 2 – 13 GHz Eleven feed for future wideband radio telescopes", 5th European Conference On Antennas and Propagation (EuCAP 2011), Rome, Italy, 11 – 15 April 2011.